

# A Physical-Layer Orchestration Framework for Open System Models of Autonomous RISs

Victor Croisfelt, *Graduate Student Member, IEEE*, Francesco Devoti, *Member, IEEE*,  
Fabio Saggese, *Member, IEEE*, Vincenzo Sciancalepore, *Senior Member, IEEE*, Xavier Costa-Pérez, *Senior Member, IEEE*, and Petar Popovski, *Fellow, IEEE*

**Abstract**—To obviate the control of reconfigurable intelligent surfaces (RISs) and related overhead, recent works envisioned the concept of autonomous RISs: Intelligent devices capable of autonomously deciding their reflection states. This paradigm is enabled by hybrid RIS (HRIS), a hardware solution that integrates sensing and channel estimation (CHEST) capabilities, enabling autonomous operation. Autonomous RISs operate independently alongside other network entities, promoting open communication system models for RISs. However, this autonomy introduces a significant challenge: How to schedule the operation of the autonomous Reconfigurable Intelligent Surface (RIS) over time and frequency to minimize its impact on the network? This paper introduces a physical layer (PHY) orchestration framework within a massive multiple-input multiple-output (mMIMO) network to address this challenge. Our framework highlights an engineering trade-off termed the “autonomous RIS trade-off,” which examines the performance implications of autonomy. Through mathematical analysis and numerical results, we describe the HRIS feasibility region, illustrating the conditions under which autonomous RISs are viable when properly deployed.

**Index Terms**—Reconfigurable intelligent surface (RIS), intelligent reflective surface (IRS), hybrid reflective intelligent surface (HRIS), massive multiple-input multiple-output (MIMO).

## I. INTRODUCTION

RECONFIGURABLE intelligent surface (RIS) is an emerging technology with a significant role on the research agenda towards 6G [1], [2]. Typically, RIS refers to a grid of elements, or meta-atoms, that manipulates electromagnetic waves beyond classical Snell’s law. For example, configuring the phase shifts of each RIS element, known as a *configuration*, allows arbitrary changes to the reflection angle of an incoming wave [3]. Recently, this technology has enabled a new vision where numerous nearly passive, low-complexity RISs can be deployed in wireless networks, offering partial control over the propagation environment [4]. The benefits of RIS-assisted wireless networks include improved communication performance, reduced electromagnetic-field exposure, and many others [1], [2]. However, a major obstacle to the practical viability of these networks is the overhead from channel estimation (CHEST) required to acquire channel state

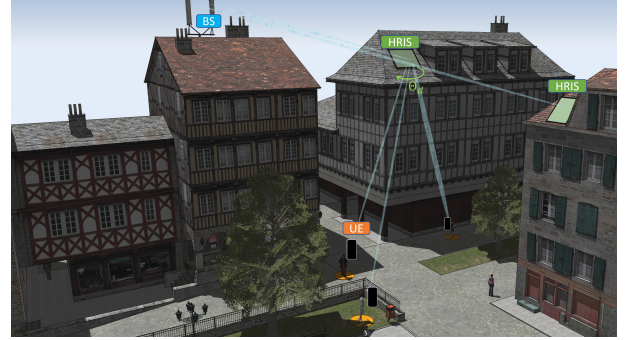


Fig. 1: Open system models of autonomous RISs where multiple HRISs enhance communication performance without an explicit control channel.

information (CSI) between the base station (BS) and user equipments (UEs) due to the passive nature of RISs [5]. Further overhead can arise from dedicated and reliable real-time signaling to control the RIS operations [6]–[8].

To mitigate these overheads, researchers advocate for using *autonomous* RISs [9], *i.e.*, RISs that can operate independently of the BS. A key enabler of autonomous RIS technology is the hybrid reconfigurable intelligent surface (HRIS), which features additional hardware like radio frequency (RF) power detectors and chains [9]. This allows the HRIS to both reflect incoming waves and sense the environment, earning it the designation of *hybrid*. Pioneering hardware solutions for HRISs are proposed in [10]–[14]. Structurally, HRISs sit between fully passive RISs and relays: They can receive RF signals but cannot transmit them [9], [15]. Throughout the remainder of this paper, we will use the term autonomous RIS to refer to the technology, and HRIS to refer to the hardware solution that implements it; we refer to standard RIS technology, where the RIS is nearly passive and controlled by another network entity, often the BS, as *non-autonomous RIS*.

Deploying HRISs transforms the network into an *open system model*, as illustrated in Fig. 1. In this model, HRISs autonomously enhance communication between the BS and UEs without needing dedicated control from the BS, which often handles CHEST and control signaling by leveraging its higher processing capabilities to make network decisions [1]. Notably, HRISs can still potentially exploit *opportunistic coordination* with network devices by monitoring the data and control channels they use. This open system model remains effective regardless of whether the HRIS is deployed by the same

V. Croisfelt, F. Saggese, and P. Popovski are with Aalborg Universitet, 9220 Aalborg, Denmark. F. Devoti and V. Sciancalepore are with NEC Laboratories Europe, 69115 Heidelberg, Germany. X. Costa-Pérez is with i2cat, ICREA, and NEC Laboratories Europe, 08034 Barcelona, Spain. This work was supported by the Villum Investigator grant “WATER” from the Velux Foundation, Denmark, by the EU H2020 RISE-6G project under grant agreement no. 101017011, and by the EU SNS JU INSTINCT project under grant agreement no. 101139161. Corresponding author email: vcr@es.aau.dk.

network operator as the BS or by a third party. Researchers have proposed that an HRIS must support and switch between at least two *operation modes* at the physical (PHY) layer to facilitate this functionality [12], [13]: *i) Probe mode*, the HRIS probes the environment to estimate CSI of the BS and UEs locally; *ii) Reflection mode*, the HRIS autonomously adjusts its configuration, so-called *reflection configuration*, using the locally estimated CSI to optimize communication performance. Despite the benefits of reducing overhead, autonomous RIS have drawbacks. Firstly, the higher hardware cost is a major concern when designing HRISs. Secondly, we have observed an autonomy-related issue: An autonomous RIS must intelligently manage when and how it performs operations, as its actions can significantly impact the shared propagation environment with other network entities. This dual nature can potentially lead to autonomous RISs negatively affecting network performance rather than enhancing it. In the case of HRISs, adjustments made during probe mode to estimate local CSI can unpredictably alter channel conditions. This can render the CSI at the BS outdated, thereby reducing communication performance instead of enhancing it. This undesired phenomenon, known as *probing distortion*, arises because the network and HRIS share the same time-frequency resources and operate in parallel. This underscores the need for a framework to efficiently schedule or *orchestrate* HRIS operations.

In this paper, building on the 5G standard [16] and recent developments in HRIS hardware [12]–[14], we investigate the PHY-layer orchestration of an HRIS within an massive multiple-input multiple-output (mMIMO) network to evaluate the practical feasibility of HRISs. The mMIMO technology is recognized as a pivotal facilitator for 5G and beyond and is actively undergoing deployment [17]. It typically works in time-division duplex (TDD) mode, which organizes the time-frequency resources in *coherence blocks*. Each coherence block is scheduled with two different *operation phases* over time [15]: 1) CHEST phase, where the BS estimates the CSI regarding the UEs, and 2) Communication (COMM) phase, where communication occurs between the BS and the UEs relying on spatial multiplexing techniques. We propose a PHY-layer orchestration framework that specifies *a)* how the HRIS operation modes are organized concerning the simultaneous network operation phases, and *b)* how the network designer or an intelligent controller can evaluate when the HRIS has to switch between its operation modes to avoid compromising the network performance. Our proposed framework enables us to mathematically analyze and numerically evaluate the impact on network performance resulting from the automation of the RIS as a function of the HRIS hardware complexity.

#### A. Related works

The RIS technology enhances wireless network performance cost-effectively by reconfiguring the propagation environment using low-complexity and low-cost hardware [18]. RISs are used, in [19], to enhance the wireless service coverage area, in [20], to improve the spectral efficiency (SE) by enhancing the channel quality for UEs experiencing poor channel conditions, in [21], to enhance interference mitigation schemes,

while, in [22], to break the channel reciprocity and reduce the effect of pilot contamination often present in mMIMO networks. However, as aforementioned, the presence of RISs introduces significant challenges regarding their integration in the network architecture, their orchestration [23], and how to conduct CHEST, which require specialized solutions to ensure optimal network performance [24], [25].

A network layer framework for controlling multiple non-autonomous RISs has been introduced in [26], where the RIS control is done by leveraging a software-defined network approach; [27] proposes an approach based on neural networks in a similar setting. [28], [29] discuss the technical challenges related to integrating RIS technology in the existing network architecture. In [29], RIS devices and orchestrating components are placed in the open RAN (ORAN) architecture framework. Notably, standardization efforts to push RIS technology into 6G standards are currently ongoing [30], [31]; but, they are still in the preliminary phase. At the time of writing, there is still a need for further validating interfaces and components for embedding and orchestrating RIS devices from the network layer perspective. Nevertheless, our work does not delve into network-layer orchestration of RISs as we focus on an autonomous RIS that operates independently.

The passive nature of non-autonomous RISs makes the CHEST procedure challenging [1], [2], [24]. This issue is aggravated by the large number of RIS elements, which increases the complexity of CHEST and reduces its accuracy, leading to reliance on imperfect or outdated CSI [25]. In [32]–[35], methods to acquire the CSI at the BS are proposed for RIS-assisted networks. In [36]–[38], the authors analyzed the performance of RIS-assisted mMIMO networks under the consideration of imperfect CSI, different precoding and combining techniques, and different ways to optimize the configuration at the RIS by using either instantaneous or statistical CSI acquired at the BS. In [39], the authors provide a solution to improve the performance of such a network for the case of mobile UEs in the presence of outdated CSI. However, in all these works, it is assumed that the BS controls the RIS with negligible overhead and idealized precision, perfectly adapting its functionalities to the network's operations over time-frequency resources. This assumption avoids considering resource disputes and impairments and neglects the impact of non-autonomy on performance metrics. Only recently have papers begun addressing the latter [6]–[8].

Autonomous RIS alleviates the control overhead and the CHEST problem by having relevant CSI being estimated locally [12]–[14], [40], [41]. In [42], a compressive sensing approach is proposed to reconstruct the full CSI from a subset of active elements at the HRIS, while in [43], the pilot signals are processed to estimate CSI. However, those methods do not analyze the impact on the network operation phases occurring in parallel to the HRIS operation modes. Given that, the closest works to ours are [12], [13], [44], where an HRIS has been optimized to assist the ongoing communication. But these works only consider the COMM phase of the network while assuming perfect CSI knowledge. To our knowledge, the PHY-layer orchestration of an HRIS in network operations has not yet been explored in the literature. This is crucial for assessing

its practical feasibility, especially in contemporary network topologies like mMIMO, as considered in this work.

### B. Contributions

The primary focus of this paper is to address the question: *Is autonomous RIS truly a feasible technology?* In pursuit of this, our main contributions are:

- We propose a PHY-layer orchestration framework conciliating the HRIS operation modes and the mMIMO operation phases within a coherence block by following two design principles: *a)* the HRIS should probe for UEs during the CHEST phase; *b)* the HRIS should transition to the reflection mode while the CHEST phase is still in progress. This design choice enables a seamless integration of autonomous HRIS, at the price of *probing distortion*.
- We design and mathematically analyze the performance of HRIS operations for two types of HRIS hardware architectures [9]: A low-complexity power detector (PD)-enabled and a more complex digital signal processing (DSP)-enabled, representing the two extremes of processing power and cost.
- We analytically characterize the performance of HRIS-assisted networks and explain how probing distortion can adversely affect network performance. This leads to the definition of the “autonomous RIS trade-off,” which balances the communication performance boost provided by the HRIS in reflection mode against the degradation caused by reduced CSI quality at the BS due to probing distortion when the HRIS is in probe mode. Achieving an optimal balance involves adjusting the relative duration of the HRIS reflection mode during the CHEST phase enabling fine-tuning of network performance.

Guided by our analytical results, our numerical findings show that HRIS-assisted networks outperform classical mMIMO systems in specific regions, referred to as the *HRIS feasibility region*, of the relative duration of the HRIS reflection mode during the CHEST phase regardless of the hardware architecture, in a typical suburban mMIMO setting. These results affirm the effectiveness of our orchestration method and suggest that autonomous RIS, implemented here as HRISs, can be viable in certain environments if well-designed.

**Paper Outline:** The remainder of the paper is organized as follows. Section II describes an HRIS-aided mMIMO system. Section III presents an overview of the proposed framework and sets the basic nomenclatures and notations. In Section IV, we firstly introduce two HRIS architectures: the PD-based and the DSP-based. Then, we design the HRIS operation modes, taking into account the specific characteristics of both architectures and analyzing their performance. In Section V, we analytically study the impact of the HRIS on the mMIMO network performance using our proposed orchestration framework. Section VI numerically evaluates the performance of the designed HRIS operation modes and the autonomous RIS trade-off by evaluating the network performance. In Section VII, we discuss practical considerations about the framework and give our conclusions.

**Notations:** Vectors and matrices are in bold lowercase and uppercase letters, respectively. The  $ij$ -th element of a matrix  $\mathbf{X}$  is  $[\mathbf{X}]_{i,j}$ ; the  $i$ -th element of a vector  $\mathbf{y}$  is  $y_i$ .

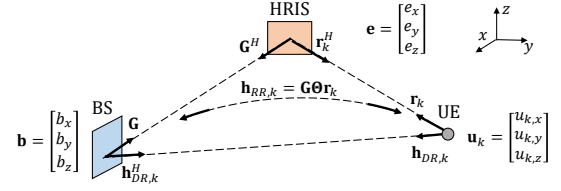


Fig. 2: Geometrical representation of the considered single-cell mMIMO network including a BS, an HRIS, and a UE.

Complex conjugate, matrix transpose, Hermitian transpose, and diagonal matrix operators are denoted as  $(\cdot)^*$ ,  $(\cdot)^T$ ,  $(\cdot)^H$ ,  $\text{diag}(\cdot)$  respectively.  $\|\cdot\|_2$  denotes the  $\ell_2$ -norm. The inner product between  $\mathbf{x}$  and  $\mathbf{y}$  is  $\langle \mathbf{x}, \mathbf{y} \rangle$ , while  $\circ$  is the Hadamard product. Integer sets are represented by calligraphic letters, e.g.,  $\mathcal{A}$  with cardinality  $|\mathcal{A}| = A$ , whereas  $\mathbb{N}$ ,  $\mathbb{R}$  and  $\mathbb{C}$  denote the sets of natural, real, and complex numbers respectively. The operators  $\Re(\cdot)$  and  $\Im(\cdot)$  return the real and the imaginary part of a number, respectively. The conditional probability distribution function (PDF) is denoted as  $p(x; E)$  for the random variable  $x$  given the event  $E$ . The exponential distribution with parameter  $\zeta$  is  $\text{Exp}(\zeta)$ , and  $Q_{\chi_n^2}(x)$  denotes the right-tail distribution of a central  $\chi_n^2$ -distributed random variable  $x$  with  $n$  degrees of freedom, while  $Q_{\chi_n^2(\mu)}(x)$  represents a non-central one, with non-centrality parameter  $\mu$ . Complex Gaussian distribution with mean  $\mu$  and variance  $\sigma^2$  is denoted as  $\mathcal{CN}(\mu, \sigma^2)$ . We use  $O(\cdot)$  for big-O notation.

## II. SYSTEM MODEL

Consider a single-cell mMIMO network where an BS equipped with a uniform linear array (ULA) of  $M$  antennas simultaneously serves  $K$  single-antenna UEs that are already scheduled, referred to as *active* UEs.<sup>1</sup> We further denote as  $K_{\max}$  the maximum number of UEs that can be supported by the network. Based on the Plug&Play approach [12], [13], a network operator deploys an HRIS to autonomously enhance the propagation conditions, where the network operator deploying the HRIS can be different to the one controlling the BS. The HRIS is comprised of  $N = N_x N_z$  elements arranged as a uniform planar array (UPA), where  $N_x$  and  $N_z$  denote the number of elements along the  $x$ - and  $z$ -axis, respectively. To simplify notation, we introduce the sets  $\mathcal{M}$ ,  $\mathcal{K}$ , and  $\mathcal{N}$  to index BS antennas, UEs, and HRIS elements, respectively. The network operates following a TDD protocol, where the time-frequency domain is sliced into *coherence blocks* of  $\tau_c$  channel uses or samples indexed by  $\mathcal{T}_c$  [17]. Wireless transmissions occur at a carrier frequency  $f_c$  with wavelength  $\lambda$ .

### A. HRIS model

The HRIS can simultaneously absorb and reflect different portions of the impinging signals. The coupling parameter  $\eta \in [0, 1]$  determines the fraction of the received power reflected by the HRIS to the environment; hence, the amount

<sup>1</sup>Scheduling UEs in the presence of an HRIS is related to the RIS-assisted initial access problem [45], [46], and it is out of the scope of this paper. However, during scheduling, we ensure that active UEs are not only served by the HRIS so they can still be spatially separable.

of power absorbed is given by  $1 - \eta$  [14].<sup>2</sup> Let  $\Theta = \text{diag}([e^{j\theta_1}, \dots, e^{j\theta_N}]^T)$  be a configuration with  $\theta_n \in [0, 2\pi]$  denoting the phase shift impressed by the  $n$ -th HRIS element. According to [12], both reflected and absorbed signals are subject to the configuration  $\Theta$ . As illustrated in Fig. 2 and focusing on the uplink (UL) direction, the equivalent BS-UE channel  $\mathbf{h}_k \in \mathbb{C}^M$  for the  $k$ -th UE can be written as

$$\mathbf{h}_k(\Theta) = \mathbf{h}_{\text{DR},k} + \mathbf{h}_{\text{RR},k}(\Theta), \quad (1)$$

where  $\mathbf{h}_{\text{DR},k} \in \mathbb{C}^M$  is the **direct** channel and  $\mathbf{h}_{\text{RR},k} \in \mathbb{C}^M$  is the **reflected** channel for  $k \in \mathcal{K}$ . The reflected channel  $\mathbf{h}_{\text{RR},k}$ , as the equivalent channel  $\mathbf{h}_k$ , is a function of the configuration  $\Theta$  and can be written in terms of the HRIS-UE channel  $\mathbf{r}_k \in \mathbb{C}^N$  and the BS-HRIS channel  $\mathbf{G} \in \mathbb{C}^{M \times N}$ .

Below, we define the concept of a subblock to help us make assumptions on how the HRIS operates.

**Definition 1** (Subblock). *We let a subblock be a group of samples within the same coherence block. We denote as  $\mathcal{T} \subseteq \mathcal{T}_c$  a subblock. Subblocks are indexed by  $s$ , which takes values from an index set  $\mathcal{S}$  that indexes partitions of samples of size  $|\mathcal{T}|$  from  $\mathcal{T}_c$ . In the special case that a subblock comprises a single sample, we have  $s \in \mathcal{T}_c$  since  $|\mathcal{T}| = 1$ .*

**Assumption 1** (HRIS configuration change). *We assume that the HRIS can change its configuration  $\Theta$  on a subblock basis. We denote as  $\Theta[s]$  the configuration impressed by the HRIS at the  $s$ -th subblock for  $s \in \mathcal{S}$ .*

The above assumption aligns with the current development of the RIS technology. Indeed, an HRIS requires a time ranging from microseconds to milliseconds to change its configuration [47], which depends on how the HRIS is built and might correspond to the duration of some samples [7]. As a consequence of the above assumption, the equivalent channel also changes on a subblock basis. Eq. (1) can be rewritten as:

$$\mathbf{h}_k[s] = \mathbf{h}_{\text{DR},k} + \mathbf{h}_{\text{RR},k}[s], \quad (2)$$

where  $\mathbf{h}_{\text{DR},k}$  is not affected by the HRIS configuration change.

### B. Channel models

Here, we present the channel models for the scenario of interest. We assume a block-fading model [17], where  $\tau_c$  is selected so the channel responses are constant and frequency flat within a coherence block. To simplify the presentation, we describe the channel model for a single UE  $k \in \mathcal{K}$  and a single coherence block. To get rid of the  $[s]$  notation in this subsection, we further assume that the HRIS impresses the same configuration  $\Theta$  over the entire block duration.

Denote as  $\mathbf{b} \in \mathbb{R}^3$ ,  $\mathbf{e} \in \mathbb{R}^3$ , and  $\mathbf{u}_k \in \mathbb{R}^3$  the locations of the BS center, the HRIS center, and the  $k$ -th UE, respectively. The position of the  $m$ -th BS antenna is  $\mathbf{b}_m \in \mathbb{R}^3$  for  $m \in \mathcal{M}$ , while of the  $n$ -th HRIS element is  $\mathbf{e}_n \in \mathbb{R}^3$  for  $n \in \mathcal{N}$ . The inter-antenna and inter-element distances of the BS and the HRIS arrays are set to  $\lambda/2$ . Let  $\mathbf{a}_B(\mathbf{p}) \in \mathbb{C}^M$  and  $\mathbf{a}_H(\mathbf{p}) \in \mathbb{C}^N$

denote the BS and HRIS array response vectors towards a generic location  $\mathbf{p} \in \mathbb{R}^3$ , respectively. The  $n$ -th element of  $\mathbf{a}_H(\mathbf{p})$  is [12]

$$[\mathbf{a}_H(\mathbf{p})]_n \triangleq e^{j\langle \mathbf{k}(\mathbf{p}, \mathbf{e}), (\mathbf{e}_n - \mathbf{e}) \rangle}, \text{ with } \mathbf{k}(\mathbf{p}, \mathbf{e}) \triangleq \frac{2\pi}{\lambda} \frac{\mathbf{p} - \mathbf{e}}{\|\mathbf{p} - \mathbf{e}\|_2}, \quad (3)$$

being  $\mathbf{k}(\mathbf{p}, \mathbf{e}) \in \mathbb{R}^3$  the wave vector. The BS steering vector  $\mathbf{a}_B(\mathbf{p})$  is derived similarly with  $\mathbf{b}, \mathbf{b}_m$  instead of  $\mathbf{e}, \mathbf{e}_n$ , respectively. Next, the pathloss model between two generic locations  $\mathbf{p}, \mathbf{q} \in \mathbb{R}^3$  is defined as [12]

$$\gamma(\mathbf{p}, \mathbf{q}) \triangleq \gamma_0 \left( \frac{d_0}{\|\mathbf{p} - \mathbf{q}\|_2} \right)^\beta, \quad (4)$$

where  $\gamma_0$  is the channel power gain at a reference distance  $d_0$  and  $\beta$  is the pathloss exponent. We assume that the direct BS-UEs channels are under pathloss exponent  $\beta_B$ , while BS-HRIS and HRIS-UEs channels suffer from pathloss exponent  $\beta_H$ . This is a valid assumption since the HRIS is often placed in such a way that its paths towards the BS and the UEs are less obstructed than the path connecting the BS to the UEs [48].

Focusing on the UL direction, we assume an independent and identically distributed (i.i.d.) Rician fading model for the BS-UE channel,  $\mathbf{h}_{\text{DR},k}$ , and for the HRIS-UE channel,  $\mathbf{r}_k$ , while the BS-HRIS channel,  $\mathbf{G}$ , is assumed to be line-of-sight (LoS) dominant, and hence deterministic. The latter assumption is valid if the HRIS is deployed to have a strong LoS towards the BS, which is often the case due to the flexibility of deployment of the HRIS [48]. However, no such assumption can be made on the links between the UEs and the BS/HRIS, justifying the Rician modeling. Thus, we have

$$\mathbf{h}_{\text{DR},k} \sim \mathcal{CN}(\bar{\mathbf{h}}_{\text{DR},k}, \sigma_{\text{DR}}^2 \mathbf{I}_M), \text{ and } \mathbf{r}_k \sim \mathcal{CN}(\bar{\mathbf{r}}_k, \sigma_{\text{RR}}^2 \mathbf{I}_N), \quad (5)$$

where  $\bar{\mathbf{h}}_{\text{DR},k}$  and  $\bar{\mathbf{r}}_k$  are the LoS components, while  $\sigma_{\text{DR}}^2$  and  $\sigma_{\text{RR}}^2$  are the relative power of the non-line-of-sight (NLoS) components for the BS-UE channel and for the HRIS-UE channel, respectively. Based on (3) and (4), the LoS components are

$$\begin{aligned} \bar{\mathbf{h}}_{\text{DR},k} &= \sqrt{\gamma(\mathbf{b}, \mathbf{u}_k)} \mathbf{a}_B(\mathbf{u}_k), \quad \bar{\mathbf{r}}_k = \sqrt{\gamma(\mathbf{u}_k, \mathbf{e})} \mathbf{a}_H(\mathbf{u}_k), \\ \text{and } \mathbf{G} &= \sqrt{\gamma(\mathbf{b}, \mathbf{e})} \mathbf{a}_B(\mathbf{e}) \mathbf{a}_H^H(\mathbf{b}). \end{aligned} \quad (6)$$

Accordingly, the reflected channel results in

$$\mathbf{h}_{\text{RR},k} = \sqrt{\eta} \mathbf{G} \mathbf{O} \mathbf{r}_k \sim \mathcal{CN} \left( \sqrt{\eta} \mathbf{G} \mathbf{O} \bar{\mathbf{r}}_k, \eta \gamma(\mathbf{b}, \mathbf{e}) N \sigma_{\text{RR}}^2 \mathbf{Q} \right), \quad (7)$$

where  $\mathbf{Q} = \mathbf{a}_B(\mathbf{e}) \mathbf{a}_B^H(\mathbf{e})$  is a covariance matrix with ones in the diagonal and off-diagonal elements capturing the BS antenna correlation evaluated at the HRIS center,  $\mathbf{e}$ . The equivalent BS-UE channel can be obtained by substituting the above in (2).

### III. A PHY-LAYER ORCHESTRATION FRAMEWORK

In this section, we present our proposed PHY-layer orchestration framework, illustrated in Fig. 3. First, we detail the operation phases of an mMIMO network and the modes of an HRIS, highlighting the need for an orchestration framework. Second, we justify our design choices for developing our framework. Finally, we introduce the mathematical notation to analyze the proposed framework.

<sup>2</sup>Note that the coupling parameter  $\eta$  depends on the HRIS hardware design and cannot be tuned dynamically, but it can be engineered for particular scopes and applications during the manufacturing of the HRIS elements [11], [14].



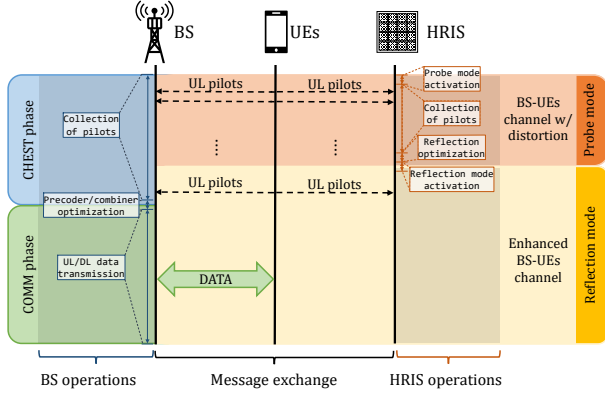


Fig. 3: Temporal evolution of the proposed PHY-layer orchestration framework. The BS alternates between two operational phases following mMIMO: 1) channel estimation (CHEST) and 2) communication (COMM) while the HRIS autonomously alternates between two modes: i) probe and ii) reflection.

#### A. Network operation overview and motivation

In a given coherence block, the network operates according to the following *operation phases* [17]. 1) CHEST phase: The UEs transmit *UL pilot signals* so that the BS can perform CHEST and estimate the CSI. Based on channel reciprocity implied by the TDD operation, the estimated CSI at the BS side holds for both downlink (DL) and UL directions. Using this estimated CSI, the BS can compute spatial multiplexing techniques such as transmit precoding and receiver combining. For simplicity, we assume that this computation does not incur any time overhead. 2) COMM phase: This phase comprises the transmission of DL and UL data traffic, where the BS spatially separates the UEs based on the computed spatial techniques.

While the network operation phases run, the HRIS *autonomously* assists the network as an open system since there is no dedicated control designed for the operation of the HRIS that is performed by the BS. Only minimal control information is exchanged: The HRIS listen to usual control channels – e.g., PDCCH in 5G NR [16] – to obtain synchronization and data frame information. Therefore, the HRIS can synchronize its operations as a standard UE, but without the need of explicitly informing the BS of its operations. The HRIS alternates between the following two *operation modes* in a given coherence block [12], [13]. i) Probe mode: The purpose of this mode is for the HRIS to probe the environment for active UEs in the surrounding area, being served by the BS at the current coherence block,<sup>3</sup> and to estimate their HRIS-UEs channels.<sup>4</sup> Note that the HRIS can also exploit the channel reciprocity resulting from the TDD operation and, consequently, it can estimate the CSI in the UL direction only and extrapolate it to

<sup>3</sup>Through standard control channels, the BS can inform the HRIS about active UEs. However, the HRIS must still probe for these UEs to obtain their CSI and self-configure accurately. Of course, if the UEs are static and their channels as well (flat-fading), the HRIS can carry probe less frequently.

<sup>4</sup>In principle, the HRIS also wishes to estimate the CSI of the BS-HRIS channel. However, under the assumption of static BS and HRIS (see Section II-B), the coherence time of the BS-HRIS channel is longer than the HRIS-UEs channels [49]. This allows us to consider perfect knowledge of the BS-HRIS channel at the HRIS, which can be obtained beforehand by listening to synchronization/pilot signals periodically sent by the BS.

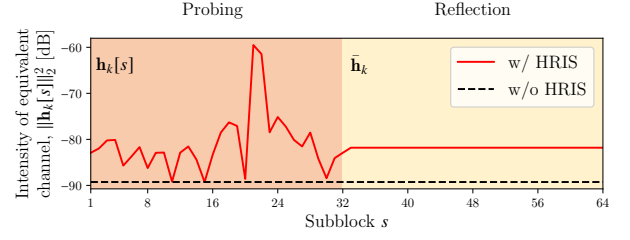


Fig. 4: Example of the evolution of the intensity of an equivalent BS-UE channel  $\mathbf{h}_k[s]$  in (2) over a coherence block of 64 subblocks, assuming the HRIS changes its configuration every subblock (Assump. 1). Channel power *can vary* significantly in probe mode but remains *stable* in reflection mode. The BS aims to perform CHEST when the channel stabilizes, while the HRIS needs to probe during this phase to utilize UL pilot signals, potentially causing *probing distortion* that affects CSI quality at the BS.

the DL direction.<sup>5</sup> ii) Reflection mode: Based on the estimated CSI, the HRIS optimizes and loads a *reflection configuration* enhancing the UEs' propagation conditions to maximize a given network key performance indicator (KPI). Note that this optimization depends on the probing performance in acquiring the CSI, ultimately linking the effectiveness of the reflection mode to the performance of the probe mode. As before, we also assume that the computation of the reflection configuration does not incur any time overhead. The HRIS should keep the reflection configuration loaded during the COMM phase, until the next coherence block starts.

*Motivation for orchestration*: Since the HRIS needs to switch between two operation modes within a coherence block, it can affect the network operation phases in an undesirable way. To illustrate this, Fig. 4 shows how the power or intensity of the equivalent BS-UE channel, defined in (1), can evolve over a given coherence block according to the HRIS switching between its modes. We observe distinct channel properties under each mode. In probe mode, the channel power *can vary* as the HRIS can periodically change its configuration to probe for UEs. Conversely, during reflection mode, the channel remains *stable* as the HRIS maintains the reflection configuration. It is important to note that mMIMO relies on the assumption that the channel estimated during the CHEST phase remains consistent during the COMM phase [17]. However, the channel variations observed in probe mode, as illustrated in Fig. 3, challenge this assumption and can degrade the performance of spatial multiplexing. Therefore, strategically orchestrating the HRIS operation modes to align with network operation phases becomes imperative.

#### B. Design choices and the autonomous RIS trade-off

For a given coherence block, Fig. 3 summarizes the operations of the BS, HRIS, and UEs and their temporal evolution according to the proposed orchestration framework. To effectively benefit from the HRIS deployment, we pragmatically arrange its operations according to the operation phases of

<sup>5</sup>We assume channel reciprocity is perfectly achieved by using carefully designed hardware and/or calibration algorithms [17] to allow us to focus on discussing the main ideas behind our proposed framework. Future research can explore what happens if channel reciprocity is violated by/at the HRIS.

the mMIMO system by proposing two design rules. First, the HRIS probe mode must partially overlap with the CHEST phase. The reason behind this choice is that the HRIS can take advantage of the UL pilot signals to probe for the UEs and subsequently estimate their CSI. Second, the HRIS must be in reflection mode before the end of the CHEST phase and during the entire COMM phase. By imposing the start of the reflection mode to occur during the CHEST phase, we ensure that the BS can collect a certain number of samples of the stable equivalent BS-UE channels (see Fig. 4).

Following these two choices, we observe that the HRIS eventually *distorts* the estimated CSI at the BS during the CHEST phase. We define this distortion as follows.

**Definition 2** (Probing distortion). *The probing distortion is the distortion introduced by the HRIS into the estimated CSI at the BS as a consequence of the fact that the HRIS probe mode can alter the propagation environment during the network CHEST phase (see Fig. 4). This may lead to an unreliable CSI at the BS, which may result in an incorrect spatial separation of the UEs, potentially hindering network performance.*

To mitigate probing distortion, the HRIS should minimize its probing duration and swiftly transition to the reflection mode. However, reducing the probing duration may reduce the probing performance, *i.e.*, the HRIS may acquire poor local CSI, eventually leading to a reduced performance boost during the reflection mode. This compromise gives rise to the so-called *autonomous RIS trade-off*, informally defined below.

**Definition 3** (Autonomous RIS trade-off). *The autonomous RIS trade-off balances the probing distortion and the HRIS-assisted network performance by controlling the duration of the HRIS probe mode. The goal is to characterize the region where the HRIS-assisted network performance is higher than the network performance without assistance. This region is called the HRIS feasibility region.*

This trade-off is a direct consequence of the autonomy of the HRIS operation. We aim to study this trade-off to understand the feasibility of HRIS in practice.

### C. Detailed network operation

We now introduce the basic mathematical machinery needed to analyze our orchestration framework. Figure 5 illustrates how the coherence block is sliced simultaneously into the different network operation phases and HRIS operation modes. Specifically, we let  $\tau_{\text{chest}}$  and  $\tau_{\text{comm}}$  be the number of samples comprising the network CHEST and COMM phases, respectively, such that  $\tau_c = \tau_{\text{chest}} + \tau_{\text{comm}}$ . The COMM phase can be further divided into  $\tau_d$  and  $\tau_u$  samples for DL and UL data traffic, respectively; that is,  $\tau_{\text{comm}} = \tau_d + \tau_u$ . Simultaneously, we let  $\tau_{\text{prob}} \leq \tau_{\text{chest}}$  and  $\tau_{\text{ref}}$  be the number of samples in which the HRIS operates in probe and reflection modes, respectively, with  $\tau_c = \tau_{\text{prob}} + \tau_{\text{ref}}$ . For a given coherence block and during connection establishment, the BS performs a UL pilot assignment  $p(i) : \mathcal{K} \mapsto \mathcal{T}_p$ , where each UE is assigned to a pilot signal in a deterministic way. In other words,  $p(i) \in \mathcal{T}_p$  represents the index of the pilot signal assigned to UE  $i \in \mathcal{K}$ .

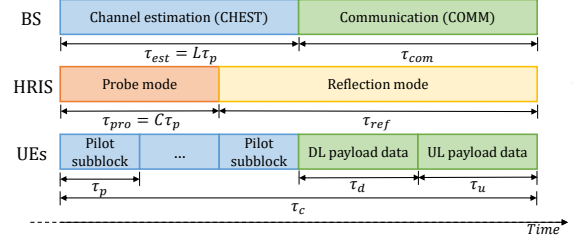


Fig. 5: Coherence block organization for each network entity.

Each pilot  $\Phi_t \in \mathbb{R}^{\tau_p}$  spans for  $\tau_p$  samples. The pilots are selected from a pilot codebook  $\Phi \in \mathbb{R}^{\tau_p \times \tau_p}$  with columns representing the  $\tau_p$  pilots enumerated by the index set  $\mathcal{T}_p \subset \mathcal{T}_c$  with  $|\mathcal{T}_p| = \tau_p$ . We assume the following about the pilot codebook.

**Assumption 2** (Orthogonal pilot codebook). *The pilot codebook contains orthogonal sequences, such that  $\Phi_t^H \Phi_{t'} = \tau_p$  if  $t = t'$  and  $\Phi_t^H \Phi_{t'} = 0$  for  $t \neq t'$ ,  $\forall t, t' \in \mathcal{T}_p$ . In particular, we assume  $\Phi = \sqrt{\tau_p} \mathbf{I}_{\tau_p}$ . To avoid multi-user interference during the CHEST phase, the maximum number of UEs supported by the network is equal to the pilot length, *i.e.*,  $K_{\max} = \tau_p$ .*

Assumption 2 is based on the rule-of-thumb for selecting the number of pilots described in [17]. We say a pilot signal is *active* if assigned to a UE. Otherwise, a pilot signal is *inactive*. We further assume that the HRIS knows  $\Phi$  and, hence,  $\tau_p$  and  $K_{\max}$ .<sup>6</sup>

Due to our orchestration framework and the orthogonality of the pilot signals, an issue emerges if we take the duration of the CHEST phase to be equal to the pilot length, that is,  $\tau_{\text{chest}} = \tau_p$ . To see it, consider the following example.

**Example 1.** *Consider that  $K = K_{\max} = \tau_p = 2$  and that  $\tau_{\text{chest}} = \tau_p$ . Assume that UE 1 is assigned to the pilot signal  $[\sqrt{2}, 0]^T$  and UE 2 to  $[0, \sqrt{2}]^T$ . Because of the probing distortion, we want  $0 < \tau_{\text{prob}} < \tau_{\text{chest}}$ ; hence, we choose  $\tau_{\text{prob}} = 1$ . In this case, the HRIS would receive just the first entries of the pilot signals sent by the UEs. Since the first entry of UE 2's pilot signal is 0, the HRIS would be able to probe only UE 1 no matter what UE 2 does.*

We assume the following *pilot repetition strategy* to solve the above problem, which consequently defines the duration of the CHEST phase.<sup>7</sup>

**Assumption 3** (Pilot repetition – CHEST duration). *Each UE re-transmits its pilot signal for  $L > 1$  times such that  $\tau_{\text{chest}} = L\tau_p$ . We refer to each of the pilot repetitions as a pilot subblock following Definition 1, which is indexed by the set  $\mathcal{L}$  with  $\mathcal{L}$  being a partition of the set  $\mathcal{T}_p$ . We index variables that occur on a pilot-subblock basis by introducing an  $[l]$  in front of it with  $l \in \mathcal{L}$ .*

<sup>6</sup>Remark that also this information does not need a dedicated control channel: The HRIS can listen to the information regularly broadcasted by the BS on the PDCCCH to learn the pilot codebook [16].

<sup>7</sup>Another solution to this problem would be to design a non-orthogonal pilot codebook. However, we leave this aspect to future works, and we consider Assumption 2 to better focus on the functionality of our proposed framework and the fundamental insights of the autonomous RIS trade-off.

This assumption allows us to effectively accommodate the HRIS probing within the CHEST phase while also being able to control the duration of the former and avoiding the problem seen in Example 1.<sup>8</sup> Based on the above assumption, we define the probing duration as follows.

**Definition 4** (Probing duration). *The probing duration is an integer multiple of the pilot length  $\tau_p$  satisfying  $0 < \tau_{\text{prob}} \leq \tau_{\text{chest}}$ . Hence, the HRIS probe mode spans for  $\tau_{\text{prob}} = C\tau_p$  with  $1 \leq C \leq L$  being the number of pilot subblocks in which the HRIS probes. The pilot subblocks where the HRIS probes can be collected in the subset  $C \subseteq L$ . We index variables that occur on a pilot subblock basis but, during probing, by introducing a  $[c]$  in front of it with  $c \in C$ .*

As a consequence of the above, the portion of the coherence block that the HRIS operates in reflection mode is

$$\tau_{\text{refl}} = \tau_c - \tau_{\text{prob}} = \tau_c - C\tau_p. \quad (8)$$

We further define the following complementary quantity.

**Definition 5** (Relative reflection duration during the CHEST phase). *The duration of the HRIS being in reflection mode during the CHEST phase relative to the number of pilot subblocks can be defined as:*

$$\varpi = \frac{L - C}{L}, \text{ with } 0 \leq \varpi \leq 1, \quad (9)$$

where  $\varpi$  equals one in the absence of the HRIS probe mode and evaluates to zero when the HRIS probe mode occupies the entire duration of the CHEST phase.

**Remark 1** (HRIS feasibility region). *According to Definition 3, the region in which the use of HRIS is feasible can be defined by finding values of  $\tau_{\text{prob}} = C\tau_p$ ,  $C$ , or  $\varpi$  such that the HRIS-assisted network performance is higher than the one in which the network works alone.*

To further delineate the HRIS feasibility region, we assess the performance of its probe mode in Section IV and the network performance when assisted by the HRIS in Section V. These evaluations highlight the dependence on  $\varpi$ , which plays a crucial role in striking a balance.

#### IV. HRIS OPERATION

In this section, we detail the HRIS operation. First, we introduce two widely accepted hardware implementations of the HRIS in the literature. These architectures illustrate how the HRIS operation modes and performance are influenced by its sensing capability and cost. Second, we present the essential features constituting the probe mode. This is followed by presenting two HRIS probing strategies compliant with the two different HRIS hardware architectures. For simplicity, when deriving these procedures, we chose not to overload the notation indicating signals related to each hardware implementation. Third, we present a method to calculate the reflection

<sup>8</sup>We note that the only explicit change required in the typical mMIMO protocol to accommodate the HRIS is pilot repetition. Information signaling for this can be exchanged during a predefined setup phase without affecting the COMM phase.

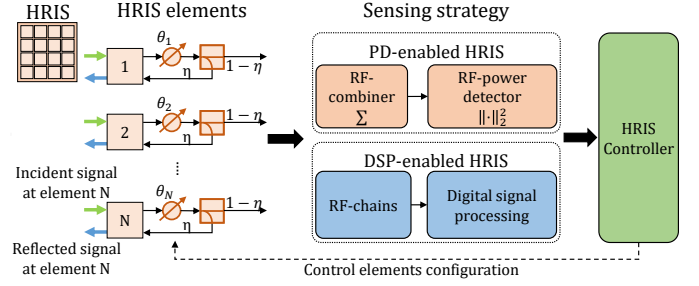


Fig. 6: PD- and DSP-enabled hardware architectures of the HRIS.

configuration when the HRIS operates in the reflection mode, common to both hardware architectures. Finally, we discuss the computational complexity of the HRIS operation modes.

#### A. HRIS hardware architectures

Fig. 6 depicts the two considered HRIS hardware architectures: PD-enabled and DSP-enabled. In both, the HRIS elements' joint reflection and absorption capabilities are realized through directional couplers, able to reflect a portion  $\eta$  and absorb  $1 - \eta$  of the incoming power [11], [14]. The two considered hardware architectures differ in how the absorbed signal is processed to extract information, as follows.

- **PD-enabled HRIS.** The HRIS hardware is characterized by a single RF chain in the absorption branch, which combines (sums) the absorbed signals at each HRIS element and feeds an RF-power detector measuring the received power [12], [13]. This hardware architecture is the most cost- and energy-efficient. However, DSP at the HRIS is limited to processing the combined received power only.

- **DSP-enabled HRIS.** The HRIS hardware is characterized by an RF chain for each element, which outputs  $N$  separated digital data streams. Thus, more powerful DSP techniques can be applied over the  $N$  acquired samples [14], at the price of a higher hardware complexity and energy consumption.

Regardless of the architecture, the HRIS switches between operation modes by activating or deactivating the sensing hardware and loading the configurations specifically designed for the probe or the reflection modes. Nevertheless, it is worth highlighting that hardware architectures impact how the probe mode is carried as we detail in the following.

#### B. Probe mode: General considerations

According to the CHEST phase described in Section III-C, the UEs transmit pilots for  $L$  pilot subblocks while the HRIS probes during  $C$  out of the  $L$  pilot subblocks. For the  $c$ -th pilot subblock, the superimposed pilot signals  $\mathbf{\Pi}[c] \in \mathbb{C}^{N \times \tau_p}$  impinging at the HRIS are

$$\mathbf{\Pi}[c] \in \mathbb{C}^{N \times \tau_p} = \sqrt{\rho} \sum_{i \in \mathcal{K}} \mathbf{r}_i \Phi_{p(i)}^T, \quad (10)$$

where  $\rho$  is the UE transmit power,  $p(i)$  denotes the pilot assigned to the  $i$ -th UE by the BS, and  $\mathbf{r}_i$  is the HRIS-UE channel of the  $i$ -th UE, as in (5). From Assumption 2, recall that at most only one UE can be associated with a pilot signal.

According to Assumption 1, we consider that the HRIS can change its configuration to help in probing for UEs. For example, the HRIS can scan the surrounding area by changing its configurations to detect signals coming from different directions. We refer to these as *probing configurations*. Based on Assumption 4, we assume the HRIS can change probing configurations on a pilot subblock basis. For mathematical tractability, we will limit ourselves to the case that a *probing configuration codebook* is available at the HRIS, which is comprised of  $C$  configurations and is denoted as

$$\Theta_P = \{\Theta_P[c] \mid c \in C\}. \quad (11)$$

In general, the HRIS needs to detect the UEs under its influence and estimate their CSI locally. Indeed, not all the active UEs may be served; for example, a UE far away from the HRIS may be active but undetectable due to the low power received and, thus, cannot be properly served by the HRIS. Therefore, we use detection theory [50] to design the HRIS probe mode. Then, the output of the detection procedure is exploited for acquiring local CSI at the HRIS. When doing so, we assume that the HRIS is unaware of the distribution of the HRIS-UEs channels,  $\mathbf{r}_i$  in (5).<sup>9</sup> Consequently, we make use of the generalized likelihood ratio test (GLRT) [50] to probe for UEs.

*Outputs of the probe mode:* At the end of the HRIS probing procedure, the HRIS has a *set of detected UEs*, denoted as  $\mathcal{K}_D$  with  $|\mathcal{K}_D| = K_D$ . To design the reflection mode, the local CSI needed by the HRIS is the angular information of the HRIS-UEs channels  $\angle \mathbf{r}_j$ , which we denote as  $\hat{\Theta}_j \in \mathbb{C}^{N \times N}$  for  $j \in \mathcal{K}_D$ , and a vector of weights  $\omega = [\omega_1, \dots, \omega_{K_D}]^T \in \mathbb{R}_+^{K_D}$  denoting the relevance of each detected UE.

Below, we provide two alternatives to conduct the HRIS probing for the respective PD-enabled and DSP-enabled HRIS hardware architectures. The design of the proposed methods can be seen as an instance of this general formulation, where the probing configuration codebook  $\Theta_P$  is designed to leverage the potential of the available HRIS hardware.

### C. PD-enabled probe mode

First, we design a probing configuration codebook suitable for a PD-enabled HRIS. We then present the corresponding probing procedure and analyze its performance based on the channel model shown in Section II-B. Finally, we define how the HRIS estimates its local CSI.

1) *Design of the probing configuration codebook:* Similar to the approach proposed in [12] and to overcome the lack of DSP capabilities, the PD-enabled HRIS probes for UEs by sweeping through probing configurations in  $\Theta_P$ . We build the probing configuration codebook to slice the 3D space into  $C$  uniform sectors of interest with  $C = C_{\text{el}} C_{\text{az}}$  being decomposed into elevation and azimuth directions, respectively. The  $n$ -th diagonal element of the  $c$ -th probing configuration is

$$[\Theta_P[c]]_{n,n} = e^{j(\mathbf{k}(\mathbf{p}[c], \mathbf{e}), (\mathbf{e}_n - \mathbf{e}))}, \quad (12)$$

<sup>9</sup>The availability of the channels distribution at the HRIS would allow better-probing performance, e.g., by relying on Bayesian tests. However, it implies additional complexity at the HRIS, which is in contrast with the core principle of being a resource-constrained device.

for  $n \in \mathcal{N}$  and  $c \in C$  where the  $c$ -th probed position is

$$\mathbf{p}[c] = [\sin \psi[c] \cos \phi[c], \sin \psi[c] \cos \phi[c], \cos \psi[c]]^T, \quad (13)$$

with elevation and azimuth angular directions being

$$\psi[c] = \frac{\pi}{C_{\text{el}}} \left( \text{mod}_{C_{\text{el}}}(c-1) + \frac{1}{2} \right) \text{ and} \quad (14)$$

$$\phi[c] = \frac{\pi}{C_{\text{az}}} \left( \frac{c-1 - \text{mod}_{C_{\text{el}}}(c-1)}{C_{\text{el}}} + \frac{1}{2} \right). \quad (15)$$

2) *Probing procedure and performance analysis:* Consider a given pilot subblock  $c \in C$  where the  $c$ -th probing configuration is loaded at the HRIS according to (12). Let  $\theta_P[c] = [e^{j\theta_1}, \dots, e^{j\theta_N}]^T \in \mathbb{C}^N$  denote the diagonal elements of  $\Theta_P[c]$ . Based on (10) and after the RF-combiner in Fig. 6, the  $c$ -th pilot subblock signal  $\mathbf{y}[c] \in \mathbb{C}^{\tau_P}$  received at the PD-enabled HRIS is

$$(\mathbf{y}[c])^T = \sqrt{1 - \eta} \sqrt{\rho} (\theta_P[c])^H \left( \sum_{i \in \mathcal{K}} \mathbf{r}_i \Phi_{p(i)}^T \right) + (\mathbf{n}[c])^T, \quad (16)$$

where  $\mathbf{n}[c] = [n_1[c], \dots, n_{\tau_P}[c]]^T \in \mathbb{C}^{\tau_P} \sim \mathcal{CN}(0, N\sigma_H^2 \mathbf{I}_{\tau_P})$  is the receiver noise at the HRIS after the RF-combiner with  $\sigma_H^2$  being the HRIS noise power, which is assumed to be i.i.d. over different subblocks.

Let us focus on the  $t$ -th pilot signal for  $t \in \mathcal{T}_P$  and the  $k$ -th UE for  $k \in \mathcal{K}$ . Based on Assumption 2, the above expression can be rewritten as

$$y_t[c] = \begin{cases} \sqrt{1 - \eta} \sqrt{\rho} \sqrt{\tau_P} (\theta_P[c])^H \mathbf{r}_k + n_t[c], & \text{if } p(k)=t \\ n_t[c], & \text{o/w.} \end{cases} \quad (17)$$

Let  $\alpha_t[c] = |y_t[c]|^2$  denote the signal after the RF-power detector in Fig. 6. Then, we have that

$$\alpha_t[c] = \begin{cases} |A_k[c]|^2 + 2\Re\{A_k[c]n_t[c]\} + |n_t[c]|^2, & \text{if } p(k)=t \\ |n_t[c]|^2, & \text{o/w,} \end{cases} \quad (18)$$

where the amplitude  $A_k$  is defined as:

$$A_k[c] = \sqrt{1 - \eta} \sqrt{\rho} \sqrt{\tau_P} (\theta_P[c])^H \mathbf{r}_k. \quad (19)$$

The PD-enabled HRIS can store and digitally process the signals  $\alpha_t[c]$ ,  $\forall t \in \mathcal{T}_P$ , to detect the UEs.

Based on the above, the PD-enabled HRIS detects if the  $k$ -th UE is in the direction probed by the  $c$ -th configuration by applying the following binary hypothesis test over each one of the pilot signals [50]:

$$\begin{aligned} \mathcal{H}_0^{(k)}[c] : \alpha_t[c] = |n_t[c]|^2 &\implies A_k[c] = 0, \\ \mathcal{H}_1^{(k)}[c] : \alpha_t[c] = |y_t[c]|^2 &\implies A_k[c] \neq 0, \end{aligned} \quad (20)$$

where the null hypothesis  $\mathcal{H}_0^{(k)}[c]$  denotes the case in which the  $k$ -th UE was not assigned to the  $t$ -th pilot signal, that is,  $p(k) \neq t$  and, consequently,  $A_k[c] = 0$ . Note that the test is realized over the amplitude  $A_k[c]$ , which is not directly observed from  $\alpha_t[c]$ , as seen in (18). Hence, we need to estimate  $A_k[c]$  from  $\alpha_t[c]$ . But, the best we can do is to employ a least-squares (LS) estimator and estimate  $|A_k[c]|^2$  from  $\alpha_t[c]$  since we cannot undo the combining operation performed by the RF-power detector. Let  $f_{\text{LS}}(A_k[c])$  denote



this LS estimate. The LS estimator for  $|A_k[c]|^2$  from  $\alpha_t[c]$  is

$$f_{\text{LS}}(A_k[c]) = \alpha_t[c]. \quad (21)$$

Thus, the PD-enabled HRIS decides  $\mathcal{H}_1^{(k)}[c]$  if [50, p. 200]:

$$\frac{p(\alpha_t[c]; f_{\text{LS}}(A_k[c]), \mathcal{H}_1^{(k)}[c])}{p(\alpha_t[c]; \mathcal{H}_0^{(k)}[c])} > \epsilon_s, \quad (22)$$

where  $\epsilon_s$  is a threshold parameter. We give the performance of the PD-enabled HRIS probing below.

**Corollary 1.** *An approximated closed-form expression of the performance of the PD-based probe mode given by the test in (20) can be found in the asymptotic case where the number of HRIS elements  $N \rightarrow \infty$  as [50]:*

$$P_D^{(k)}[c] = e^{-\frac{1}{2N\sigma_H^2}(\epsilon'_s - \alpha_t[c])} \text{ and } P_{\text{FA}}^{(k)}[c] = e^{-\frac{1}{2N\sigma_H^2}\epsilon'_s}, \quad (23)$$

where  $P_D^{(k)}[c]$  and  $P_{\text{FA}}^{(k)}[c]$  are the probabilities of detection and false alarm for detecting the  $k$ -th UE in the  $c$ -th subblock, respectively. The threshold parameter  $\epsilon'_s$  is proportional to  $\epsilon_s$  in (22).

*Proof.* The proof is given in Appendix A.  $\square$

It is important to note that the above performance measures overestimate the real performance due to approximations made. Moreover, the probability of detection is a random variable that varies on a coherence-block basis due to its dependence on  $\alpha_t[c]$ .

After performing the test in (20) over all pilot signals  $t \in \mathcal{T}_p$ , the HRIS stores the detected UEs in the set  $\mathcal{K}_D[c] = \{k \in \mathcal{K} | \mathcal{H}_1^{(k)}[c] \text{ is true}\} \subseteq \mathcal{K}$ . The above process is repeated over all pilot subblocks  $c \in \mathcal{C}$ , and the HRIS aggregates the detection results over all the pilot subblocks. Finally, the HRIS stores all the detected UEs and the corresponding probing configurations with the highest received power as

$$\mathcal{K}_D = \bigcup_{c \in \mathcal{C}} \mathcal{K}_D[c] \text{ and } c_j^* = \arg \max_{c \in \mathcal{C}} \alpha_{p(j)}[c], \forall j \in \mathcal{K}_D. \quad (24)$$

3) *HRIS CSI estimation:* The PD-enabled HRIS can not explicitly estimate the HRIS-UE channels  $\mathbf{r}_j$ 's of the detected UEs  $j \in \mathcal{K}_D$  since it has as input only the power measures of the pilot signals, as in (18). Therefore, the best the PD-enabled HRIS can do is to use the probing configuration with the highest received power as an estimate of the local CSI of the  $j$ -th UE. The HRIS local CSI acquired by the probing mode for the  $j$ -th UE is

$$\hat{\mathbf{\Theta}}_j = \mathbf{\Theta}_P[c_j^*], \quad (25)$$

where  $c_j^*$  comes from (24). We also compute weights  $\omega_j$  to measure the importance of the  $j$ -th UE to the HRIS with respect to (w.r.t.) the other UEs as

$$\omega_j = \frac{\sqrt{\alpha_{p(j)}[c_j^*]}}{\sum_{j' \in \mathcal{K}_D} \sqrt{\alpha_{p(j')}[c_{j'}^*]}}. \quad (26)$$

#### D. DSP-enabled probe mode

In this part, we proceed as in the previous subsection.

1) *Design of the probing configuration codebook:* With the DSP-enabled HRIS hardware, the HRIS has more DSP capabilities available and can process the received signals coming from all elements simultaneously. Because of this, we observe that the HRIS can always reverse back the effect of the impressed probing configuration  $\mathbf{\Theta}_P[c]$  digitally at the price of increased computational effort, which involves multiplying the received signal by  $\mathbf{\Theta}_P[c]^{-1}$  at a given sample that comprises the  $c$ -th pilot subblock for  $c \in \mathcal{C}$ . For convenience, we then assume that  $\mathbf{\Theta}_P[c] = \mathbf{I}_N, \forall c \in \mathcal{C}$ .

2) *Probing procedure and performance analysis:* Based on (10) and the above probing configuration design, the  $c$ -th pilot subblock signal  $\mathbf{Y}_c \in \mathbb{C}^{N \times \tau_p}$  received at the DSP-enabled HRIS is

$$\mathbf{Y}[c] = \sqrt{1-\eta}\sqrt{\rho} \sum_{i \in \mathcal{K}} \mathbf{r}_i \Phi_{p(i)}^\top + \mathbf{N}[c], \quad (27)$$

where  $\mathbf{N}[c] \in \mathbb{C}^{N \times \tau_p}$  is the receiver noise matrix with columns distributed according to  $\mathbf{n}_t[c] \sim \mathcal{CN}(\mathbf{0}, \sigma_H^2 \mathbf{I}_N)$ . Unlike the PD-enabled HRIS, the DSP-enabled HRIS can process the received signal over the elements-dimension,  $N$ , the pilot-dimension,  $\tau_p$ , and the pilot-subblock-dimension,  $c$ .

As before, let us focus on the  $t$ -th pilot signal for  $t \in \mathcal{T}_p$  and the  $k$ -th UE for  $k \in \mathcal{K}$ . We first start by processing over the pilot dimension. The HRIS de-correlates the received signal w.r.t. the  $t$ -th pilot signal as:

$$\tilde{\mathbf{y}}_t[c] = \mathbf{Y}[c] \Phi_t^* = \begin{cases} \sqrt{1-\eta}\sqrt{\rho}\tau_p \mathbf{r}_k + \tilde{\mathbf{n}}_t[c], & \text{if } p(k) = t \\ \tilde{\mathbf{n}}_t[c], & \text{o/w,} \end{cases} \quad (28)$$

where  $\tilde{\mathbf{n}}_t[c] \sim \mathcal{CN}(\mathbf{0}, \tau_p \sigma_H^2 \mathbf{I}_N)$ . Next, to combat noise, the HRIS can average up the de-correlated received signals over pilot subblocks as

$$\check{\mathbf{y}}_t = \frac{1}{C} \sum_{c \in \mathcal{C}} \tilde{\mathbf{y}}_t[c] = \begin{cases} \sqrt{1-\eta}\sqrt{\rho}\tau_p \mathbf{r}_k + \check{\mathbf{n}}_t, & \text{if } p(k) = t \\ \check{\mathbf{n}}_t, & \text{o/w,} \end{cases} \quad (29)$$

where  $\check{\mathbf{n}}_{p(k)} \sim \mathcal{CN}(\mathbf{0}, \frac{\tau_p \sigma_H^2}{C} \mathbf{I}_N)$ . The above signal can be further averaged over the element dimension, yielding in

$$\bar{\mathbf{y}}_t = \frac{1}{N} \sum_{n \in \mathcal{N}} \check{\mathbf{y}}_{t,n} = \begin{cases} \sqrt{1-\eta}\sqrt{\rho}\tau_p \bar{\mathbf{r}}_k + \bar{\mathbf{n}}_t, & \text{if } p(k) = t \\ \bar{\mathbf{n}}_t, & \text{o/w,} \end{cases} \quad (30)$$

where  $\bar{\mathbf{r}}_k = (1/N) \sum_{n \in \mathcal{N}} \mathbf{r}_{k,n}$  and  $\bar{\mathbf{n}}_{p(k)} \sim \mathcal{CN}(\mathbf{0}, \frac{\tau_p \sigma_H^2}{NC} \mathbf{I}_N)$ . After all these pre-processing steps, the DSP-enabled HRIS can store and digitally process the signals  $\bar{\mathbf{y}}_t, \forall t \in \mathcal{T}_p$ , to detect the UEs.

We use (30) and let  $A_t = \sqrt{1-\eta}\sqrt{\rho}\tau_p \bar{\mathbf{r}}_k$  be the complex magnitude observed if the  $k$ -th UE transmitted the  $t$ -th pilot signal, that is,  $p(k) = t$ . The DSP-enabled HRIS detects the  $k$ -th UE by applying the following binary detection problem over each one of the pilot signals [50]:

$$\begin{aligned} \mathcal{H}_0^{(k)} : \bar{\mathbf{y}}_t &= \bar{\mathbf{n}}_t, A_t = 0, \\ \mathcal{H}_1^{(k)} : \bar{\mathbf{y}}_t &= A_t + \bar{\mathbf{n}}_t, A_t \neq 0, \end{aligned} \quad (31)$$

where, as before, the null hypothesis  $\mathcal{H}_0^{(k)}$  denotes the case in which the  $k$ -th UE was not assigned to the  $t$ -th pilot signal. Unlike the PD-enabled HRIS, the detection is now independent on the pilot subblocks due to the higher DSP capability of

the DSP-enabled HRIS. Thus, the DSP-enabled HRIS decides  $\mathcal{H}_1^{(k)}$  if [50, p. 484]:

$$\mu = \frac{|\bar{y}_{p(k)}|^2}{\frac{\tau_p \sigma_H^2}{2NC}} > \epsilon_s, \quad (32)$$

where  $\epsilon_s$  is a threshold parameter. We give the performance of the DSP-enabled HRIS probing below.

**Corollary 2.** *An approximated closed-form expression of the performance of the DSP-enabled HRIS probe mode given by the test given in (32) can be found as [50, p. 484]*

$$P_D^{(k)} = Q_{\chi_4^2(\mu)}(\epsilon_s) \text{ and } P_{FA}^{(k)} = Q_{\chi_4^2}(\epsilon_s), \quad (33)$$

where  $P_D^{(k)}$  and  $P_{FA}^{(k)}$  are the probabilities of detection and false alarm for detecting the  $k$ -th UE, respectively, and  $\mu$  is defined in (32).

*Proof.* The proof follows directly from [50, p. 484].  $\square$

Unlike Corollary 1, the above does not rely on approximations, and the performance is now independent of the pilot subblocks,  $c$ . However, the probability of detection is a random variable over coherence blocks due to its dependence on  $\mu$ .

After performing the test in (32) over all pilot signals  $t \in \mathcal{T}_p$ , the HRIS stores the detected UEs in the set  $\mathcal{K}_D = \{t | \mathcal{H}_1^{(t)} \text{ is true}, t \in \mathcal{T}_p\} \subseteq \mathcal{K}$ .

3) *HRIS CSI estimation:* Unlike the PD-enabled case, the DSP-enabled HRIS can explicitly estimate the angular information of the HRIS-UEs channels  $\angle \mathbf{r}_j$  for  $j \in \mathcal{K}_D$  by exploiting the signal in (29) to perform such estimation. We now describe such an estimation process for the  $j$ -th detect UE assigned to the  $t$ -th pilot signal with  $p(j) = t$  for  $j \in \mathcal{K}_D$ . Let  $\mathbf{a}_j = \sqrt{1 - \eta} \sqrt{\rho} \tau_p \mathbf{r}_j$  be the received complex magnitude containing useful information. Let  $\boldsymbol{\theta}_j = \angle \mathbf{r}_j \in \mathbb{C}^N$  denote the angular information of the HRIS-UE channel, which we are interested in estimating. From (29), we observe that the angular information contained in  $\mathbf{a}_j$  is equivalent to the one contained in  $\mathbf{r}_j$ , that is,  $\angle \mathbf{a}_j \equiv \angle \mathbf{r}_j$ , since  $\mathbf{a}_j$  is proportional to  $\mathbf{r}_j$ . The estimation of  $\boldsymbol{\theta}_j$  is then based on rewriting the signal in (29) as  $\check{\mathbf{y}}_t = \mathbf{a}_j + \check{\mathbf{n}}_t$ . Thus, the HRIS estimates  $\boldsymbol{\theta}_j$  as

$$\hat{\boldsymbol{\theta}}_j = \exp \left( 1j \arctan \left( \frac{\Im(\check{\mathbf{y}}_t)}{\Re(\check{\mathbf{y}}_t)} \right) \right), \quad (34)$$

where the  $\exp$  and  $\arctan$  functions are applied element-wise over the vector entries, and we use the notation  $1j$  to stress the difference between the UE index and the complex constant. The estimation error can be numerically approximated as the variance of the following  $\check{\mathbf{y}}_t \sim \mathcal{CN}(\mathbf{a}_j, (\tau_p \sigma_H^2 / C) \mathbf{I}_N)$ . The local CSI at the DSP-enabled HRIS is

$$\hat{\boldsymbol{\Theta}}_j = \text{diag}(\hat{\boldsymbol{\theta}}_j). \quad (35)$$

Again, we compute the weight  $\omega_j$  to measure the importance of the  $j$ -th UE to the HRIS w.r.t. the other UEs as

$$\omega_j = \frac{|\check{y}_{p(j)}|_2}{\sum_{j' \in \mathcal{K}_D} |\check{y}_{p(j')}|_2}. \quad (36)$$

### E. Reflection mode

In this part, we describe how the reflection configuration employed during the HRIS reflection mode is computed based on the outputs of the probe mode, *i.e.*, the local CSI given by  $\hat{\boldsymbol{\Theta}}_j$ , and  $\omega_j$ ,  $\forall j \in \mathcal{K}_D$ . These quantities are given in (25) and (26) for a PD-enabled HRIS, and in (35) and (36) for a DSP-enabled HRIS, respectively. Despite the varying outputs, the design of the reflection mode remains independent of the HRIS hardware, although performance eventually differs.

During the reflection mode, the HRIS loads a reflection configuration to assist the UL data traffic and *another* for the DL data traffic. Based on the channel reciprocity from the TDD mode and perfect calibration (see Section II), we note that the reflection configuration for the UL can be simply the complex conjugate of the one during DL. Therefore, we focus solely on designing a single reflection configuration for the UL direction. Let  $\boldsymbol{\Theta}_R$  be the UL reflection configuration. Similar to [12], our goal is to find  $\boldsymbol{\Theta}_R$  that maximizes the signal-to-noise ratio (SNR) as KPI of the detected UEs, which is given by

$$\hat{\boldsymbol{\Theta}}_R = \boldsymbol{\Theta}_B \circ \sum_{k \in \mathcal{K}_D} \omega_k \hat{\boldsymbol{\Theta}}_k^*, \quad (37)$$

where  $\mathcal{K}_D$  is the set of detected UEs and  $\boldsymbol{\Theta}_B = \text{diag}(\mathbf{a}_H(\mathbf{b}))$  denotes the CSI of the HRIS-BS channel  $\mathbf{G}$  in (6), which is assumed to be perfectly known.

We now give a way to measure how good the designed reflection configuration is. In the ideal scenario where the HRIS probe is perfect, the HRIS would use the following optimal reflection configuration, assuming all UEs are detected and their CSI is accurately estimated:

$$\boldsymbol{\Theta}_R = \boldsymbol{\Theta}_B \circ \sum_{k \in \mathcal{K}} \omega_k \text{diag}(\boldsymbol{\theta}_k)^*, \quad (38)$$

where  $\boldsymbol{\theta}_k = \exp(j \arctan(\Im(\mathbf{r}_k)/\Re(\mathbf{r}_k)))$  and  $\omega_k = \|\mathbf{r}_k\|_2 / \sum_{i \in \mathcal{K}} \|\mathbf{r}_i\|_2$ . Therefore, a general way to measure how good is the reflection mode is based on the following normalized mean-squared error (NMSE):

$$\text{NMSE}_H(\varpi) = \frac{\|\hat{\boldsymbol{\Theta}}_R - \boldsymbol{\Theta}_R\|_2^2}{\|\boldsymbol{\Theta}_R\|_2^2}, \quad (39)$$

where  $\hat{\boldsymbol{\Theta}}_R$  and  $\boldsymbol{\Theta}_R$  are the diagonals of  $\hat{\boldsymbol{\Theta}}_R$  and  $\boldsymbol{\Theta}_R$ , respectively, and  $(\varpi)$  stress that this measure depends on the probing duration, as discussed in Definition 5, while the other parameters remain fixed. Observe that  $\text{NMSE}_H(\varpi)$  already encloses the performance of the probe mode since it depends on its outputs; it also depends on the chosen HRIS hardware architecture and statistically varies over coherence blocks and noise realizations.

**Remark 2.** *We note that the weights  $\omega$ , indicating the relevance of each detected UE, can be calculated using various methods. Future research can explore alternative design choices. In this work, we focus on designing  $\omega$  based on the differences in the amplitudes of the received pilot signals, where we favor UEs closer to the HRIS; but it can also make sense to favor UEs more far apart depending on the context.*

### F. Complexity analysis: HRIS operation modes

For the PD-enabled HRIS, the RF-combiner and power detector can be implemented with analog circuitry. Thus, digital processing is made for (22), (24), and (26), yielding in a total of  $C + K_{\max}C + 3K_{\max}$  element-wise operations. The DSP-enabled HRIS performs (28), (29), (30), (32), (34), and (36), resulting in a total of  $NK_{\max}^3 + CN + K_{\max} + 3NK_{\max} + 2K_{\max}$  element-wise operations. By adding up to  $2NK_{\max}$  operations to compute the diagonal reflection configuration (37), we obtain  $O(K_{\max}(2N+C+3)+C)$  for the PD-enabled processing, and  $O(N(K_{\max}^3+5K_{\max}+C)+3K_{\max})$  for the DSP-enabled one. Hence, we observe that the complexity of a PD-enabled HRIS increases linearly with the parameters of interest, while the complexity of a DSP-enabled HRIS scales cubically with the maximum number of UEs supported by the network.

### V. NETWORK PERFORMANCE ANALYSIS

This section evaluates the network performance using our orchestration framework, as presented in Section III (see Fig. 3 for an overview). Notably, the network performance depends on the HRIS operation and hardware architecture. Nevertheless, in this section, we analyze the network performance from a general perspective by assuming a generic HRIS architecture that can be then replaced by either the PD-enabled or the DSP-enabled hardware architectures, presented in Section IV-A, or any other architecture. Our analysis follows the following steps. First, we derive the mean-squared error (MSE) of the CHEST phase that evaluates the impact of the probing distortion (see Definition 2) over the estimated CSI at the BS. Second, we present a lower bound for the SE of a UE during the COMM phase while taking into consideration the distorted estimated CSI at the BS and the HRIS reflection mode. Finally, using these results, we numerically analyze the HRIS feasibility region via the autonomous RIS trade-off (see Definition 3). For simplicity, we will assume the COMM phase includes only UL traffic, with  $\tau_d = 0$  and  $\tau_u = \tau_c - L\tau_p$ ; extending this to the DL case is straightforward.

#### A. CHEST phase

According to (1) and the CHEST phase described in Section III-C, we define the following two equivalent channels for the  $i$ -th UE:

$$\begin{cases} \mathbf{h}_{p,i}[l] = \mathbf{h}_{DR,i} + \sqrt{\eta}\mathbf{G}\mathbf{\Theta}_P[l]\mathbf{r}_i \\ \mathbf{h}_{R,i} = \mathbf{h}_{DR,i} + \sqrt{\eta}\mathbf{G}\hat{\mathbf{\Theta}}_R\mathbf{r}_i, \end{cases} \quad (40)$$

where  $\mathbf{h}_{p,i}[l]$  is the equivalent channel while the HRIS probes for pilot subblocks  $l \in \mathcal{L}$  and  $\mathbf{h}_{R,i}$  is the equivalent channel while the HRIS is in reflection mode. Recall that  $C$  is the set of pilot subblocks in which the HRIS is in probe mode (see Definition 4),  $\mathbf{\Theta}_P[l]$  is the probing configuration of the  $l$ -th pilot subblock, as in (11), and  $\hat{\mathbf{\Theta}}_R$  is the reflection configuration, as in (37).

Accordingly, the BS receives the following pilot signal  $\mathbf{Z} \in \mathbb{C}^{M \times \tau_p}$  in the pilot subblock  $l \in \mathcal{L}$ :

$$\mathbf{Z}[l] = \sqrt{\rho} \begin{cases} \sum_{i \in \mathcal{K}} \mathbf{h}_{p,i}[l] \Phi_{p(i)}^\top + \mathbf{W}[l] & \text{if } l \in C \\ \sum_{i \in \mathcal{K}} \mathbf{h}_{R,i} \Phi_{p(i)}^\top + \mathbf{W}[l] & \text{o/w,} \end{cases} \quad (41)$$

where  $\mathbf{W}[l] \in \mathbb{C}^{M \times \tau_p}$  is the BS receiver noise with i.i.d. entries according to  $\mathcal{CN}(0, \sigma_B^2)$  with  $\sigma_B^2$  being the BS noise power for  $i \in \mathcal{K}$ . The noise is also considered to be i.i.d. over pilot subblocks.

In principle, the BS aims to estimate the stable equivalent channels  $\{\mathbf{h}_{R,i}\}_{i \in \mathcal{K}}$  from the collected  $\mathbf{Z}[l]$ 's. However, this estimation process suffers from the probing distortion introduced by the  $\mathbf{h}_{p,i}[l]$ 's. Since the BS is unaware of this distortion, the BS carries out the following CHEST procedure.

**CHEST procedure:** For the sake of argument, we focus on the channel estimate of the  $k$ -th UE and assume that the UE  $k \in \mathcal{K}$  transmitted the pilot signal  $t \in \mathcal{T}_p$ , i.e.,  $p(k) = t$ . Let  $\mathbf{Z} = [\mathbf{Z}[1], \dots, \mathbf{Z}[L]] \in \mathbb{C}^{M \times L\tau_p}$  be the horizontally concatenated matrix of all pilot subblocks received by the BS. Denote as  $\Phi_{Lt} = [\Phi_t; \dots; \Phi_t] \in \mathbb{C}^{L\tau_p}$  the vector containing the  $t$ -th pilot signal repeated  $L$  times. To estimate the equivalent channel, the BS first takes the mean of the de-correlated received signals in (41), yielding in

$$\begin{aligned} \bar{\mathbf{z}}_k &= \frac{1}{L} \mathbf{Z} \Phi_{Lt}^* \\ &= \sqrt{\rho} \tau_p \frac{1}{L} \left[ \sum_{l=1}^C \mathbf{h}_{p,k}[l] + (L-C) \mathbf{h}_{R,k} \right] + \frac{1}{L} \sum_{l=1}^L \mathbf{w}_t[l], \\ &\stackrel{(a)}{=} \underbrace{\sqrt{\rho} \tau_p \left( \frac{1}{L} \sum_{l=1}^C \mathbf{h}_{p,k}[l] + \varpi \mathbf{h}_{R,k} \right)}_{=\bar{\mathbf{h}}_k} + \frac{1}{L} \sum_{l=1}^L \mathbf{w}_t[l], \end{aligned} \quad (42)$$

where  $\mathbf{w}_t[l] \sim \mathcal{CN}(\mathbf{0}, \tau_p \sigma_B^2 \mathbf{I}_M)$  is the equivalent receiver noise, and  $\bar{\mathbf{h}}_k \in \mathbb{C}^M$  represents the average channel, which includes the average of the HRIS-UE channels during probe mode (causing probing distortion) and the stable HRIS-UE channel during reflection mode that the BS aims to estimate. In (a), we have used Definition 5 that specifies the relative reflection duration during the CHEST phase in terms of pilot subblocks. Below, we provide the distorted estimated CSI at the BS based on the LS estimate of  $\bar{\mathbf{h}}_k$ .<sup>10</sup>

**Corollary 3.** The LS estimate of the channel  $\bar{\mathbf{h}}_k$  based on  $\bar{\mathbf{z}}_k$  is  $\hat{\mathbf{h}}_k = \frac{1}{\sqrt{\rho} \tau_p} \bar{\mathbf{z}}_k \sim \mathcal{CN}(\bar{\mathbf{h}}_k, \hat{\sigma}^2 \mathbf{I}_M)$ , where  $\hat{\sigma}^2 = \frac{\sigma_B^2}{L \rho \tau_p}$  denotes the variance of the estimate.

*Proof.* The proof follows [51, p. 225].  $\square$

To evaluate the CSI quality at the BS, we define the average NMSE for the  $k$ -th UE relative to its true stable channel  $\mathbf{h}_{R,k}$  – the channel of interest to be estimated – as follows:

$$\overline{\text{NMSE}}_{\text{CHEST},k} = \mathbb{E} \left\{ \frac{\|\hat{\mathbf{h}}_k - \mathbf{h}_{R,k}\|_2^2}{\|\mathbf{h}_{R,k}\|_2^2} \right\} = \frac{M \hat{\sigma}^2 + \|\bar{\mathbf{h}}_k - \mathbf{h}_{R,k}\|_2^2}{\|\mathbf{h}_{R,k}\|_2^2}, \quad (43)$$

where the expectation is taken w.r.t. noise realizations when considering the channel model introduced in Section II-B. By

<sup>10</sup>To align with the HRIS design discussed in Section IV, we assume that the BS has no prior knowledge of the channel statistics. Otherwise, Bayesian estimation methods could be employed to enhance performance further.

the definition of  $\mathbf{h}_{P,k}$  and  $\mathbf{h}_{R,k}$  in (40) and using the results of Corollary 3, the average NMSE can be rewritten as:

$$\overline{\text{NMSE}}_{\text{CHEST},k} = \frac{\frac{M}{L} \frac{\sigma_B^2}{\rho \tau_p} + \frac{\eta}{L^2} \left\| \mathbf{G} \left( \sum_{l=1}^C \mathbf{\Theta}_P[l] - C \hat{\mathbf{\Theta}}_R \right) \mathbf{r}_k \right\|_2^2}{\frac{\eta}{L^2} \left\| \mathbf{G} \hat{\mathbf{\Theta}}_R \mathbf{r}_k \right\|_2^2}, \quad (44)$$

where the first term of the numerator accounts for the *true LS estimation error*, that is, if  $\mathbf{h}_{R,k}$  was to be estimated without probing distortion. The second term of the numerator evaluates the effect of *HRIS probing distortion*, following Definition 2. Observe that the  $\overline{\text{NMSE}}_{\text{CHEST},k}$  is a random variable concerning UE positions, channel realizations, and the HRIS hardware with their respective probing approaches. The derivations to obtain (43) and (44) are considered straightforward. Note that (44) can also be written w.r.t.  $\varpi$  by using (9).

**Remark 3** (Measuring probing distortion). *From Definition 2 and eq. (44), we can draw three main conclusions: First, there would be no probing distortion if the probing phase did not exist, i.e.,  $C = 0$  or  $\varpi = 1$ , which is self-evident. Therefore, minimizing the probing duration is desirable. Second, probing distortion would also be absent if the probing configurations were identical to the reflection configuration,  $\mathbf{\Theta}_P[l] = \hat{\mathbf{\Theta}}_R, \forall l \in \mathcal{L}$ . However, this knowledge is unattainable before the probe mode is conducted.<sup>11</sup> Third, the estimation error is maximized when the HRIS probing occupies the entire CHEST phase, i.e.,  $C = 1$  and  $\varpi = 0$ . Thus, an alternative way to measure the probing distortion is through*

$$\text{probe dist. level} = \frac{\left\| \sum_{l=1}^C \mathbf{\Theta}_P[l] - C \hat{\mathbf{\Theta}}_R \right\|_F^2}{\left\| \hat{\mathbf{\Theta}}_R \right\|_F^2}, \quad (45)$$

which measures how different the probing and reflection configurations are. This measure is independent of the channel realizations, but it depends on the HRIS hardware architecture and the design of the probe and reflection modes.

**Remark 4** (Complexity analysis: CHEST comparison). *Here, we compare the complexity of the CHEST procedure between non-autonomous RIS and autonomous RIS. When controlling an RIS, the BS must estimate channel coefficients for all UE-RIS and RIS-BS channels to optimize the RIS configuration [6]. Without leveraging on specific channel structures, this involves estimating  $K_{\max}(M + N + MN)$  channel coefficients, requiring transmission of at least  $2K_{\max} + N$  pilot signals [52]. In contrast, in an HRIS-assisted network, the BS only needs to estimate  $K_{\max}M$  channel coefficients of the equivalent channel with the transmission of  $L \geq K_{\max}$  pilot signals.*

## B. COMM phase

During the COMM phase, the BS exploits the distorted estimated CSI in Corollary 3 to help decode the messages

<sup>11</sup>If the UEs are static and their channel is frequency-flat, probing may not be necessary, and we can eliminate probing distortion by relying on existing information. However, in scenarios with mobile UEs and fading channels, more frequent probing is necessary. One potential approach to mitigate probing distortion is to implement intelligent probing strategies using outdated location information as a guide. Future research could further optimize these probing methods.

sent by the UEs while the HRIS is in the reflection mode. Let  $\mathbf{v}_k$  denote the receive combining vector for the  $k$ -th UE with  $k \in \mathcal{K}$ . By focusing on the UL and a particular sample of the  $\tau_u$  samples, the BS estimates the signal sent by the  $k$ -th UE as follows [17]:

$$\hat{s}_k = \mathbf{v}_k^H \mathbf{h}_{R,k} s_k + \sum_{i \in \mathcal{K}, i \neq k} \mathbf{v}_k^H \mathbf{h}_{R,i} s_i + \mathbf{v}_k^H \mathbf{o}, \quad (46)$$

where  $\mathbf{h}_{R,k}$  is defined in (40),  $s_j \sim \mathcal{CN}(0, \rho)$  is the random data signal transmitted by the  $j$ -th UE with  $j \in \mathcal{K}$ , and  $\mathbf{o} \sim \mathcal{CN}(\mathbf{0}, \sigma_B^2 \mathbf{I}_M)$  is the BS receiver noise. Thus, the instantaneous UL signal-to-interference-plus-noise ratio (SINR) of the  $k$ -th UE is

$$\text{SINR}_k^{\text{UL}} = \frac{|\mathbf{v}_k^H \mathbf{h}_{R,k} s_k|^2}{\sum_{i \in \mathcal{K}, i \neq k} |\mathbf{v}_k^H \mathbf{h}_{R,i} s_i|^2 + |\mathbf{v}_k^H \mathbf{o}|^2}. \quad (47)$$

Hence, the instantaneous UL SE of the  $k$ -th UE can be calculated as

$$\text{SE}_k^{\text{UL}} = \frac{\tau_u}{\tau_{\text{chest}} + \tau_u} \log_2 \left( 1 + \text{SINR}_k^{\text{UL}} \right). \quad (48)$$

We can use the use-and-then-forget (UatF) bound to estimate the above measure, resulting in the following Corollary replicated from [17, p. 302].

**Corollary 4.** *The UL SE of the  $k$ -th UE can be lower bounded on average w.r.t. signal and noise realizations as*

$$\underline{\text{SE}}_k^{\text{UL}} = \frac{\tau_u}{\tau_{\text{chest}} + \tau_u} \log_2 \left( 1 + \underline{\text{SINR}}_k^{\text{UL}} \right), \quad (49)$$

where

$$\underline{\text{SINR}}_k^{\text{UL}} = \frac{\rho \mathbb{E} \left\{ \left| \mathbf{v}_k^H \mathbf{h}_{R,k} \right|^2 \right\}}{\rho \sum_{i=1, i \neq k}^K \mathbb{E} \left\{ \left| \mathbf{v}_k^H \mathbf{h}_{R,i} \right|^2 \right\} + \mathbb{E} \left\{ \left| \mathbf{v}_k^H \mathbf{o} \right|^2 \right\}}. \quad (50)$$

The above corollary applies to different choices of  $\mathbf{v}_k$ , such as the maximum-ratio (MR) scheme, where  $\mathbf{v}_k = \hat{\mathbf{h}}_k$  [17].

## C. Autonomous RIS trade-off

Based on the performance of the HRIS-assisted network given by Corollaries 3 and 4, we can now more formally discuss the autonomous RIS trade-off, first presented in Definition 3. Let  $\bar{\mathbf{h}}_{P,k} = \frac{1}{L} \sum_{l=1}^C \mathbf{h}_{P,k}[l]$ . From Corollary 3, we rewrite the distorted CSI as

$$\hat{\mathbf{h}}_k \sim \mathcal{CN} \left( \bar{\mathbf{h}}_{P,k} + \varpi \mathbf{h}_{R,k}, \hat{\sigma}^2 \mathbf{I}_M \right). \quad (51)$$

From the above, we can note that the adverse effect of the probing distortion is to shift the mean of the estimated CSI away from  $\mathbf{h}_{R,k}$  – the CSI of interest to the BS, and this value is only attainable when the HRIS refrains from probing, that is when  $C = 0$  or  $\varpi = 1$ . Since the receive combining vector  $\mathbf{v}_k$  is a function of the estimated CSI, this shift will also inevitably influence it. Consequently, from (9), we can express  $\mathbf{v}_k$  as:

$$\mathbf{v}_k = \bar{\mathbf{v}}_{P,k} + \varpi \mathbf{v}_{R,k}, \quad (52)$$

where  $\bar{\mathbf{v}}_{P,k}$  represents the part of the receive combining vector that is misled by the probing distortion and  $\mathbf{v}_{R,k}$  is the desired part of the receive combining vector.



We aim to assess the influence of (52) on the network performance outlined in Corollary 4. While the impact manifests in the SINR, our focus shifts to the signal-to-interference ratio (SIR) for analytical convenience. Utilizing (52) and the triangle inequality property of the absolute value, the SIR of the  $k$ -th UE can be written as:

$$\underline{\text{SIR}}_k^{\text{UL}} \leq \frac{\mathbb{E}\left\{\left|\bar{\mathbf{v}}_{\text{P},k}^{\text{H}} \mathbf{h}_{\text{R},k}\right|^2\right\} + \varpi^2 \mathbb{E}\left\{\left|\mathbf{v}_{\text{R},k}^{\text{H}} \mathbf{h}_{\text{R},k}\right|^2\right\}}{\sum_{i=1, i \neq k}^K \mathbb{E}\left\{\left|\bar{\mathbf{v}}_{\text{P},k}^{\text{H}} \mathbf{h}_{\text{R},i}\right|^2\right\} + \varpi^2 \sum_{i=1, i \neq k}^K \mathbb{E}\left\{\left|\mathbf{v}_{\text{R},k}^{\text{H}} \mathbf{h}_{\text{R},i}\right|^2\right\}}. \quad (53)$$

In the ideal case of zero probing distortion, this SIR is:

$$\underline{\text{SIR}}_k^{\text{UL}} \leq \frac{\mathbb{E}\left\{\left|\mathbf{v}_{\text{R},k}^{\text{H}} \mathbf{h}_{\text{R},k}\right|^2\right\}}{\sum_{i=1, i \neq k}^K \mathbb{E}\left\{\left|\mathbf{v}_{\text{R},k}^{\text{H}} \mathbf{h}_{\text{R},i}\right|^2\right\}}. \quad (54)$$

To show the negative impact of probing distortion and show that (54) is an upper bound of (53), we compare (53) to (54) and obtain the following result.

**Corollary 5.** *One notable drawback of an autonomous HRIS is the resulting probing distortion, which can reduce the numerator of the SIR as defined in (53), while simultaneously increasing its denominator. This means probing distortion can elevate the interference power among UEs and decrease their effective power for a given receive combining vector  $\mathbf{v}$ . This effect is stochastic, as it depends on the UE's channel state, which is influenced by both fading and the UE's position and is dependent on the design of the probe mode.*

*Proof.* The proof can be found in Appendix B.  $\square$

Based on this result, along with Corollaries 1 and 2, we can formally establish the autonomous RIS trade-off. This trade-off shows that probing distortion can degrade network performance while reducing probing distortion eventually impacts probing performance and the eventual relevance of deploying an HRIS. By tuning  $\varpi$ , we can balance these two effects. Additionally, we observe that  $\underline{\text{SIR}}_k^{\text{UL}}$  can result in a HRIS-assisted network performance inferior to that without HRIS. In the next section, we substantiate this finding numerically. This is attributed to probing distortion elevating the interference term (in the denominator) at a rate significantly higher than the rate at the effective power (in the numerator) is reduced.

## VI. NUMERICAL RESULTS

We now numerically evaluate the performance of the HRIS operation modes and the HRIS-assisted network performance when using our orchestration framework by analyzing the autonomous trade-off.<sup>12</sup>

### A. Simulation setup

Table I reports the simulation parameters employed, which are motivated by the suburban scenario introduced in [17] with a system bandwidth of 20 MHz. The parameters are subject

to change during the numerical evaluation. In particular, the pathloss multiplicative constant is set to  $\gamma_0 = 1$  to observe better the effect of distance from BS-UEs and RIS-UEs and their respective differences in pathloss exponents. The HRIS is located at the origin of a two-dimensional Cartesian system. The BS is placed at the second quadrant 1 km away from the HRIS at  $135^\circ$ . The UEs are randomly placed within a ring at the first quadrant. The inner radius of the ring is set to 900 m while the outer radius is set to 1 km. This scenario represents the case in which edge-UEs are assisted by the HRIS. The NLoS relative powers  $\sigma_{\text{DR}}^2$  and  $\sigma_{\text{RR}}^2$  are chosen in such a way that the NLoS powers are on average 10% of the corresponding LoS ones. The BS receiver noise  $\sigma_{\text{B}}^2 = -94$  dBm comprises the thermal noise over a system bandwidth of 20 MHz and a noise figure of 7 dB in the receiver hardware. The quality of the HRIS hardware is considered to be worse than the one at the BS, having a noise figure of 10 dB [53], and resulting in  $\sigma_{\text{H}}^2 = -91$  dBm. We have set the maximum number of UEs,  $K_{\text{max}}$  to be equal to the number of UEs,  $K$ , and, consequently, the number of pilots,  $\tau_p$  (Assump. 2). Moreover, we assume that the CHEST phase takes  $\tau_{\text{chest}} = 64$  samples, half of the coherence interval of  $\tau_c = 128$  samples [17]. Therefore, we set  $L = \frac{64}{\tau_p} = 16$  pilot subblocks.<sup>13</sup>

### B. Performance of HRIS operation

We start by evaluating the performance of the HRIS probe mode. To model the fact that UEs may not be active, we assume that at each coherence block, each UE has a probability of 50% to be active, that is, to participate in a given coherence block. Figure 7 shows the performance of the HRIS probe mode in terms of the probability of detection,  $P_{\text{D}}$  for different choices of probabilities of false alarm,  $P_{\text{FA}}$ . We use Corollaries 1 and 2 to find values of the threshold to perform the respective tests given  $P_{\text{FA}}$ . As expected, we can observe that the probability of detection degrades as either the fraction of power absorbed by the HRIS,  $1 - \eta$ , decreases or the relative reflection duration during CHEST,  $\varpi$ , increases since the number of probing subblocks  $C$  decreases (see Definition 5). We also observe that the DSP-enabled HRIS performs better than the PD-enabled HRIS, as expected. However, this performance gap reduces as  $1 - \eta$  increases. Moreover, we note some fluctuations in the performance of the PD-enabled HRIS. This is a consequence of our design choice that the probing configuration codebook changes as  $\varpi$  or  $C$  changes, as can be seen in (12). Due to the propagation conditions and because multi-user interference is not present during CHEST, we will adopt the value of  $\eta = 0.9999$  and  $P_{\text{FA}} = 10^{-2}$  for the next simulations, which enables us to focus improving the performance of the HRIS reflection mode without losing too much probing performance. Hence, the choice of  $\eta$  when manufacturing the HRIS can also be related

<sup>13</sup> The above choices ensure that the UEs have a strong enough direct link to the BS, which guarantees their spatial separability. If UEs are served only with the assistance of the HRIS, spatial separability is compromised because the channels become linearly dependent due to their combination at the RIS. This issue is a well-known problem in RIS-aided mMIMO networks [36]–[38].

<sup>12</sup>The code to reproduce the figures is available online at [this link](#).

TABLE I: Simulation Parameters

Parameter	Value	Parameter	Value	Parameter	Value
Carrier frequency, $f_c$	28 GHz	HRIS pathloss, $\beta_H$	2	BS pathloss, $\beta_B$	3.76
Number of BS antennas, $M$	64	NLoS relative power, $\sigma_{DR}^2, \sigma_{RR}^2$	$9.07 \cdot 10^{-9}, 1.12 \cdot 10^{-7}$	Number of pilots, $\tau_p$	$K$
Number of UEs, $K_{\max} = K$	4	Receive noise powers, $\sigma_H^2, \sigma_B^2$	-91, -94 dBm	Coherence block length, $\tau_c$	128 samples
Number of HRIS elements, $N$	32	UL Transmit power, $\rho$	0 dBm	HRIS reflection coefficient $\eta$	0.9999

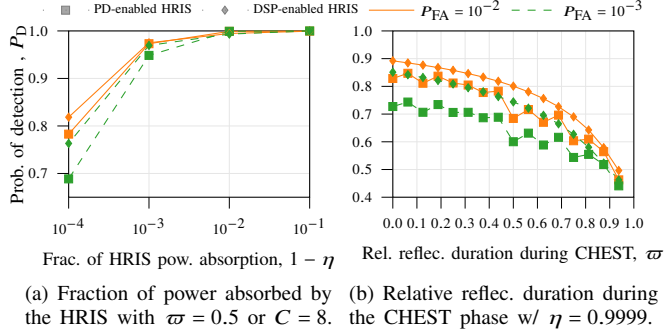


Fig. 7: Probability of detection of the HRIS probe mode when using the tests in (22) for the PD-enabled HRIS and in (32) for the DSP-enabled HRIS for different choices of probability of false alarm  $P_{FA}$  and  $K = 4$  UEs with each having a probability of 50% to be active.

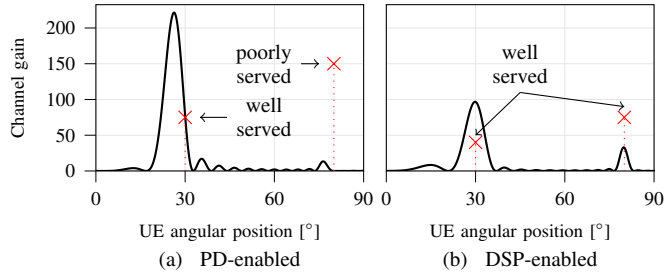


Fig. 8: Performance of the HRIS reflection mode when assuming that the  $K = 2$  UEs are detected and are active and the BS is placed 1 km from the normal line to the HRIS. In Figs. 8a and 8b, 'X' marks represent 2 UEs positioned at  $(d_k, \theta_k)$ : (10, 30°) and (20, 80°) w/  $\varpi = 0.5$  or  $C = 8$  and distances in meters.

to a target performance for the HRIS probe and reflection modes.

We now evaluate the performance of the HRIS reflection mode. In this evaluation, we operate under the assumption that the HRIS probe mode detects a total of  $K = 2$  UEs and that they transmit concurrently so that we evaluate how the quality of the local CSI at the HRIS estimated during the HRIS probe mode impacts the performance of the HRIS reflection mode. Figure 8 shows the channel gain of the UEs when the HRIS is under reflection mode. As expected, the DSP-enabled HRIS outperforms the PD-enabled HRIS in CSI estimation at the HRIS and, consequently, UE localization, resulting in gains ranging from 2-5 times higher channel gains on average. Recall that the PD-enabled HRIS relies on probing configurations to estimate CSI at the HRIS, whose number changes according to  $\varpi$  (refer to (25)).

### C. Network performance: Autonomous RIS trade-off

In Fig. 9, we show the HRIS-assisted network performance for each network phase when considering the PD-

enabled and DSP-enabled architectures and when using MR combining, that is,  $\mathbf{v}_k = \hat{\mathbf{h}}_k$ . We consider two baselines: the mMIMO baseline stands for the case that the network operates without assistance from the HRIS, while the Genie BS baseline represents the case in which the BS knows when the HRIS probes and, therefore, it just perform CHEST when the HRIS finishes probing, eliminating the probing distortion problem. In this simulation, we assume  $K = 4$  UEs that remain active across all coherence blocks. This approach enables us to concentrate on evaluating the impact of the design behind probe and reflection modes while minimizing the influence of missed detections and false alarms.

Figure 9a illustrates the impact of probing distortion on CSI quality, measured using the average NMSE metric as defined in (43) and (44). We can visually confirm Remark 3 in the figure, where the NMSE decreases as  $\varpi$  increases, allowing the BS to more frequently observe the stable CSI of interest – the equivalent channel during HRIS reflection mode in (40).

Figure 9b shows the average SE, as specified in Corollary 4. The HRIS feasibility region can be visually characterized by finding values of  $\varpi$  in which the colored curves perform better than the black curves – our gains can be up to 11% on average w.r.t. mMIMO baseline. We note that when  $\varpi \rightarrow 0$  the performance of the genie baseline tends to 0. Moreover, we also remark that a more fair performance metric to compare the genie baseline with our methods would have been based on throughput to account for the overhead introduced for the BS to be updated about the HRIS operation; however, our analysis is still valid as a worst case scenario where there is no cost in getting such coordination. In other words, this means that the genie-aided curves are unreliable and overestimate the true performance while PD-enabled and DSP-enabled curves are more reliable. From the figure, we first observe that the probing distortion, which increases when  $\varpi$  reduces, affects more the DSP-enabled approach than the PD-based one. This is because the DSP-enabled HRIS generates less variable probing distortion due to the design of the probing mode, which heavily depends on the probing configuration codebook following Remark 3. Surprisingly, this implies that lower DSP capability can be advantageous in this scenario, leading to better performance of PD-enabled HRIS under more severe probing distortion ( $\downarrow \varpi$ ). This is an unexpected finding that depends on a better understanding of the statistical characteristics of the probing distortion for each architecture. Another counter-intuitive result related to this shows that the PD- and DSP-enabled HRISs can outperform the genie baseline. The reason is that we numerically observed that probing distortion can sometimes be beneficial. It can introduce diversity among the UEs channels, differentiating their channel vectors and thereby reducing the multi-user interference term in the SINR. This effect contrasts with the detrimental findings of probing

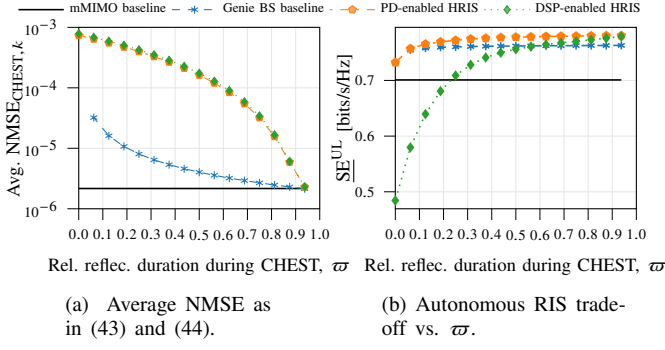


Fig. 9: Performance of an HRIS-assisted network for  $K = 4$  UEs that are always active when using MR combining,  $\eta = 0.9999$ , and  $P_{FA} = 10^{-2}$ .

distortion described in Corollary 5, whose efficacy diminishes as  $\varpi$  increases.

From the above observations, we note that probing distortion has a dual effect: it can be detrimental, as shown by Corollary 5, but it can also be beneficial by creating spatial diversity among UEs in certain regions of  $\varpi$ , which appears similar to the effect induced by spatial correlation [17].

## VII. DISCUSSION AND CONCLUSIONS

We proposed a PHY-layer orchestration framework that integrates HRIS operation modes with the operational phases of an mMIMO network. Specifically, we analyzed an extreme case where the HRIS operates autonomously, without external control. Our framework reveals a trade-off that gauges the practical feasibility of autonomous RIS. The results demonstrate that autonomous HRIS-assisted networks can surpass classical mMIMO systems when the duration of the HRIS reflection mode accounts for at least 20% of the CHEST network phase in a suburban setting. Further studies on the statistical characterization of the probing distortion models are needed to better understand the observed duality effect of probing distortion.

Many aspects of this work can be extended in future research. The analytical framework presented can be extended to scenarios in which the HRIS aids more than one operator/network autonomously. Moreover, the framework can include the performance analysis of mixed controlled/autonomous RISs, where dedicated control messages are used to control the HRIS behavior in some of the coherence blocks while letting it self-operate in others.<sup>14</sup>

### APPENDIX A PROOF OF COROLLARY 1

*Proof.* We need to get the distributions of the numerator and the denominator of the left-hand side term of (22). We start with the denominator. For the null-hypothesis in (20) with  $A_k[c] = 0$ , we note that  $\alpha_k[c] = |n_t[c]|^2$  in (18) is distributed as an exponential distribution. Hence, we obtain

$$p(\alpha_t[c]; \mathcal{H}_0^{(k)}[c]) = \text{Exp}\left(\frac{1}{2N\sigma_H^2}\right), \quad (55)$$

<sup>14</sup>We also note that developments in HRIS hardware are crucial since if we could tune  $\eta$  dynamically we could in principle circumvent probing distortion.

where we assume that the HRIS knows the noise parameter  $\sigma_H^2$  by performing some estimation process over time. Now, for the numerator, we rewrite the signal under  $\mathcal{H}_1^{(k)}$  as

$$\begin{aligned} \alpha_t[c] &= |A_k[c]|^2 + 2\Re\{A_k[c]n_t[c]\} + |n_t[c]|^2 \\ &\stackrel{(a)}{\approx} |A_k[c]|^2 + |n_t[c]|^2, \end{aligned} \quad (56)$$

where in (a), we approximate the signal by analyzing it on expectation, resulting in  $2\Re\{A_k[c]n_t[c]\}$  being 0 since the noise has zero mean. Note that its variance is still preserved in the term  $|n_t[c]|^2$ . This approximation will surely cause an overestimation of the performance since the cross-term eventually makes the decision more difficult by mixing amplitude and noise. Another motivation for such an approximation is to note that the terms  $|A_k[c]|^2$  and  $|n_t[c]|^2$  would be higher in magnitude than  $2\Re\{A_k[c]n_t[c]\}$ , where for high SNR values  $|A_k[c]|^2$  dominates; in contrast,  $|n_t[c]|^2$  dominates in low SNR. Hence, the numerator of (22) is

$$\frac{1}{2N\sigma_H^2} \exp\left(-\frac{1}{2N\sigma_H^2}(\alpha - f_{ML}(A_k[c]))\right). \quad (57)$$

By plugging (55) and (57) into (22), the HRIS decides that the  $k$ -th UE is detected in the  $c$ -th pilot subblock if

$$\alpha_t[c] \geq 2N\sigma_H^2\epsilon_s = \epsilon'_s, \quad (58)$$

which completes the proof.  $\square$

### APPENDIX B PROOF OF COROLLARY 5

*Proof.* Let the four terms that compose the  $\text{SIR}_k^{\text{UL}}$  in (53) be referred to as:

$$\text{SIR}_k^{\text{UL}} = \frac{a + \varpi^2 b}{c + \varpi^2 d}. \quad (59)$$

To support our claim that probing distorting can be detrimental, we need to show that  $a \leq b$  while  $c \geq d$  for arbitrary choices of  $\bar{\mathbf{v}}_{P,k}$ ,  $\bar{\mathbf{v}}_{R,k}$ ,  $\mathbf{h}_{R,k}$ ,  $\mathbf{h}_{R,i}$ . We first note that we must work with at least a two-dimensional space to find a solution. For the sake of argument, we choose  $\bar{\mathbf{v}}_{P,k} = [0, 1]^T$ ,  $\bar{\mathbf{v}}_{R,k} = [1, 0]^T$ ,  $\mathbf{h}_{R,k} = [0, 1]^T$ , and  $\mathbf{h}_{R,i} = [1, 0]^T$ . This yields in  $a = 0$ ,  $b = 1$ ,  $c = 1$ ,  $d = 0$ , which ends the proof.  $\square$

## REFERENCES

- [1] M. Di Renzo *et al.*, "Smart radio environments empowered by reconfigurable intelligent surfaces: How it works, state of research, and the road ahead," *IEEE Journal on Selected Areas in Communications*, vol. 38, no. 11, pp. 2450–2525, 2020.
- [2] C. Pan *et al.*, "Reconfigurable intelligent surfaces for 6G systems: Principles, applications, and research directions," *IEEE Communications Magazine*, vol. 59, no. 6, pp. 14–20, 2021.
- [3] H. Yang *et al.*, "A programmable metasurface with dynamic polarization, scattering and focusing control," *Nature, Sci Rep* 6, 35692, 2016.
- [4] E. C. Strinati *et al.*, "Wireless environment as a service enabled by reconfigurable intelligent surfaces: The RISE-6G perspective," in *Proc. Joint European Conference on Networks and Communications 6G Summit (EuCNC/6G Summit)*, 2021, pp. 562–567.
- [5] A. Zappone *et al.*, "Overhead-aware design of reconfigurable intelligent surfaces in smart radio environments," *IEEE Transactions on Wireless Communications*, vol. 20, no. 1, pp. 126–141, 2021.
- [6] E. Björnson *et al.*, "Reconfigurable intelligent surfaces: A signal processing perspective with wireless applications," *IEEE Signal Processing Magazine*, vol. 39, no. 2, pp. 135–158, 2022.

- [7] F. Saggese *et al.*, "On the impact of control signaling in ris-empowered wireless communications," *IEEE Open Journal of the Communications Society*, pp. 1–1, 2024.
- [8] —, "Control aspects for using RIS in latency-constrained mobile edge computing," in *57th Asilomar Conference on Signals, Systems, and Computers*, 2023, pp. 174–181.
- [9] M. Jian *et al.*, "Reconfigurable intelligent surfaces for wireless communications: Overview of hardware designs, channel models, and estimation techniques," *Intelligent and Converged Networks*, vol. 3, no. 1, pp. 1–32, 2022.
- [10] L. Subrt *et al.*, "Controlling the short-range propagation environment using active frequency selective surfaces," *Radioengineering*, vol. 19, no. 12, 2010.
- [11] I. Alamzadeh *et al.*, "A reconfigurable intelligent surface with integrated sensing capability," *Scientific reports*, vol. 11, no. 1, p. 20737, 2021.
- [12] A. Albanese *et al.*, "MARISA: A self-configuring metasurfaces absorption and reflection solution towards 6G," in *IEEE INFOCOM 2022 - IEEE Conference on Computer Communications*, 2022, pp. 250–259.
- [13] —, "ARES: Autonomous RIS Solution With Energy Harvesting and Self-Configuration Towards 6G," *IEEE Transactions on Mobile Computing*, 2024.
- [14] G. C. Alexandropoulos *et al.*, "Hybrid reconfigurable intelligent metasurfaces: Enabling simultaneous tunable reflections and sensing for 6G wireless communications," *IEEE Veh. Tech. Mag.*, vol. 19, no. 1, pp. 75–84, 2024.
- [15] E. Björnson *et al.*, "Intelligent reflecting surface versus decode-and-forward: How large surfaces are needed to beat relaying?" *IEEE Wireless Communications Letters*, vol. 9, no. 2, pp. 244–248, 2020.
- [16] 3GPP, "NR: Physical layer procedures for data," 3rd Generation Partnership Project (3GPP), Technical specification (TS) 38.214, 10 2022, version 15.0.0.
- [17] E. Björnson *et al.*, "Massive MIMO networks: Spectral, energy, and hardware efficiency," *Foundations and Trends® in Signal Processing*, vol. 11, no. 3–4, pp. 154–655, 2017.
- [18] J. He *et al.*, "Reconfigurable intelligent surface assisted massive MIMO with antenna selection," *IEEE Transactions on Wireless Communications*, vol. 21, no. 7, pp. 4769–4783, 2021.
- [19] A. Albanese *et al.*, "RIS-aware indoor network planning: The Rennes railway station case," in *IEEE International Conference on Communications (ICC)*. IEEE, 2022, pp. 2028–2034.
- [20] L. Wei *et al.*, "Wireless communications empowered by reconfigurable intelligent surfaces: Model-based vs model-free channel estimation," *Journal of Information and Intelligence*, vol. 1, no. 3, pp. 253–266, 2023.
- [21] J. Li *et al.*, "RIS-assisted cooperative interference alignment scheme for MIMO multi-user networks," in *IEEE International Conference on Communications (ICC)*. IEEE, 2023, pp. 889–894.
- [22] X. Luo *et al.*, "IRS-based TDD reciprocity breaking for pilot decontamination in massive MIMO," *IEEE Wireless Communications Letters*, vol. 10, no. 1, pp. 102–106, 2021.
- [23] Y. Liu *et al.*, "Reconfigurable intelligent surfaces: Principles and opportunities," *IEEE communications surveys & tutorials*, vol. 23, no. 3, pp. 1546–1577, 2021.
- [24] X. Wei *et al.*, "Channel estimation for RIS assisted wireless communications—Part I: Fundamentals, solutions, and future opportunities," *IEEE communications letters*, vol. 25, no. 5, pp. 1398–1402, 2021.
- [25] L. Wei *et al.*, "Channel estimation for ris-empowered multi-user miso wireless communications," *IEEE Transactions on Communications*, vol. 69, no. 6, pp. 4144–4157, 2021.
- [26] C. Liaskos *et al.*, "Using any surface to realize a new paradigm for wireless communications," *Communications of the ACM*, vol. 61, no. 11, pp. 30–33, 2018.
- [27] —, "End-to-end wireless path deployment with intelligent surfaces using interpretable neural networks," *IEEE Transactions on Communications*, vol. 68, no. 11, pp. 6792–6806, 2020.
- [28] —, "Software-defined reconfigurable intelligent surfaces: From theory to end-to-end implementation," *Proceedings of the IEEE*, vol. 110, no. 9, pp. 1466–1493, 2022.
- [29] E. C. Strinati *et al.*, "Reconfigurable, intelligent, and sustainable wireless environments for 6g smart connectivity," *IEEE Communications Magazine*, vol. 59, no. 10, pp. 99–105, 2021.
- [30] ETSI, "Reconfigurable Intelligent Surfaces (RIS) Use Cases, Deployment Scenarios and Requirements," ETSI, Tech. Rep. ETSI GR RIS 001 V1.1.1 (2023-04), 2023, group Report.
- [31] —, "Reconfigurable Intelligent Surfaces (RIS): Communication Models, Channel Models, Channel Estimation and Evaluation Methodology," ETSI, Tech. Rep. ETSI GR RIS 003 V1.1.1, 2023, group Report.
- [32] J. Chen *et al.*, "Channel estimation for reconfigurable intelligent surface aided multi-user mmwave mimo systems," *IEEE Transactions on Wireless Communications*, 2023.
- [33] H. Zhang *et al.*, "Channel estimation with hybrid reconfigurable intelligent metasurfaces," *IEEE Trans. Commun.*, vol. 71, no. 4, pp. 2441–2456, 2023.
- [34] A. J. Fernandes *et al.*, "Channel estimation for reconfigurable intelligent surface-assisted full-duplex mimo with hardware impairments," *IEEE Wireless Communications Letters*, 2023.
- [35] W. Shen *et al.*, "Deep learning for super-resolution channel estimation in reconfigurable intelligent surface aided systems," *IEEE Transactions on Communications*, vol. 71, no. 3, pp. 1491–1503, 2023.
- [36] Y. N. Ahmed, "Large system analysis of reflecting intelligent surface aided MIMO systems with imperfect channel state information," in *2021 28th International Conference on Telecommunications (ICT)*, 2021, pp. 1–5.
- [37] K. Zhi *et al.*, "Power scaling law analysis and phase shift optimization of RIS-aided massive MIMO systems with statistical CSI," *IEEE Transactions on Communications*, vol. 70, no. 5, pp. 3558–3574, 2022.
- [38] —, "Is RIS-aided massive MIMO promising with ZF detectors and imperfect CSI?" *IEEE Journal on Selected Areas in Communications*, vol. 40, no. 10, pp. 3010–3026, 2022.
- [39] Y. Hu *et al.*, "Serving mobile users in intelligent reflecting surface assisted massive MIMO system," *IEEE Transactions on Vehicular Technology*, vol. 71, no. 6, pp. 6384–6396, 2022.
- [40] N. T. Nguyen *et al.*, "Hybrid relay-reflecting intelligent surface-assisted wireless communications," *IEEE Transactions on Vehicular Technology*, 2022.
- [41] R. Schroeder *et al.*, "Passive RIS vs. hybrid RIS: A comparative study on channel estimation," in *IEEE 93rd Vehicular Technology Conference (VTC2021-Spring)*. IEEE, 2021, pp. 1–7.
- [42] A. Taha *et al.*, "Enabling large intelligent surfaces with compressive sensing and deep learning," *IEEE access*, vol. 9, pp. 44 304–44 321, 2021.
- [43] R. Schroeder *et al.*, "Channel estimation for hybrid RIS aided MIMO communications via atomic norm minimization," in *IEEE International Conference on Communications Workshops (ICC Workshops)*. IEEE, 2022, pp. 1219–1224.
- [44] C. Saigre-Tardif *et al.*, "A self-adaptive RIS that estimates and shapes fading rich-scattering wireless channels," *arXiv preprint arXiv:2202.10248*, 2022.
- [45] V. Croisfelt *et al.*, "A random access protocol for RIS-aided wireless communications," in *2022 IEEE 23rd International Workshop on Signal Processing Advances in Wireless Communication (SPAWC)*, 2022, pp. 1–5.
- [46] —, "Random access protocol with channel oracle enabled by a reconfigurable intelligent surface," *IEEE Transactions on Wireless Communications*, vol. 22, no. 12, pp. 9157–9171, 2023.
- [47] L. Dai *et al.*, "Reconfigurable intelligent surface-based wireless communications: Antenna design, prototyping, and experimental results," *IEEE Access*, vol. 8, pp. 45 913–45 923, 2020.
- [48] B. Xu *et al.*, "Reconfigurable intelligent surface configuration and deployment in three-dimensional scenarios," in *IEEE International Conference on Communications Workshops (ICC Workshops)*, 2021, pp. 1–6.
- [49] J. Yuan *et al.*, "Channel tracking for RIS-enabled multi-user SIMO systems in time-varying wireless channels," in *IEEE International Conference on Communications Workshops (ICC Workshops)*, 2022, pp. 145–150.
- [50] S. M. Kay, *Fundamentals of Statistical Signal Processing: Detection Theory*. Prentice Hall, 1997.
- [51] —, *Fundamentals of Statistical Signal Processing: Estimation Theory*. Prentice Hall, 1997.
- [52] Z. Wang *et al.*, "Channel estimation for intelligent reflecting surface assisted multiuser communications: Framework, algorithms, and analysis," *IEEE Trans. Wireless Commun.*, vol. 19, no. 10, pp. 6607–6620, 2020.
- [53] A. F. Molisch, *Wireless Communications*, 2nd ed. Wiley Publishing, 2011.